

Does the Hartman effect exist in triangular barriers

Qing-Ling Li(李青玲), Shuang Zheng(郑爽), and Zhi Xiao(肖智)

Citation: Chin. Phys. B, 2024, 33 (**3**): 030306. DOI: 10.1088/1674-1056/acf2fe
Journal homepage: http://cpb.iphy.ac.cn; http://iopscience.iop.org/cpb

What follows is a list of articles you may be interested in

Lie transformation on shortcut to adiabaticity in parametric driving quantum systems

Jian-Jian Cheng(程剑剑), Yao Du(杜瑶), and Lin Zhang(张林)
Chin. Phys. B, 2021, 30 (**6**): 060302. DOI: 10.1088/1674-1056/abd747

General way to define tunneling time

Zheng Shu(舒正), Xiaolei Hao(郝小雷), Weidong Li(李卫东), Jing Chen(陈京)
Chin. Phys. B, 2019, 28 (**5**): 050301. DOI: 10.1088/1674-1056/28/5/050301

Transmission time in the reflectionless complex potential

Yin Cheng (殷澄), Wang Xian-Ping (王贤平), Shan Ming-Lei (单鸣雷), Han Qing-Bang (韩庆邦), Zhu Chang-Ping (朱昌平)
Chin. Phys. B, 2014, 23 (**10**): 100301. DOI: 10.1088/1674-1056/23/10/100301

Dynamical time versus system's time in quantum mechanics

Duv san Arsenović, Nikola Burić, Dragomir Davidović, and Slobodan Prvanović
Chin. Phys. B, 2012, 21 (**7**): 070302. DOI: 10.1088/1674-1056/21/7/070302

Does the Hartman effect exist in triangular barriers

Qing-Ling Li(李青玲)[1], Shuang Zheng(郑爽)[1], and Zhi Xiao(肖智)[1,2,†]

[1] *Department of Mathematics and Physics, North China Electric Power University, Beijing* 102206, *China*
[2] *Hebei Key Laboratory of Physics and Energy Technology, North China Electric Power University, Baoding* 071000, *China*

(Received 21 May 2023; revised manuscript received 2 August 2023; accepted manuscript online 23 August 2023)

We study the phase, Larmor and dwell times of a particle scattered off triangular barriers (TBs). It is interesting that the dependences of dwell, reflective phase and Larmor times on the wave number, barrier width and height for a pair of mirror-symmetric (MS) exact triangular barriers (ETBs) are quite different, as the two ETBs have quite distinct scattering surfaces. In comparison, the dependence of the transmitted phase or Larmor times is exactly the same, since the transmitted amplitudes are the same for a pair of MS TBs. We further study the Hartman effect by defining the phase and Larmor velocities associated with the phase and Larmor times. We find no barrier width saturation effect for the transmitted and reflected times. This is indicated by the fact that all the velocities approach finite constants that are much smaller than the speed of light in vacuum for TBs with positive-slope impact faces. As for ETBs with vertical left edges, the naive velocities seem to also indicate the absence of the Hartman effect. These are quite distinct from rectangular barriers and may shed new light on the clarification of the tunneling time issues.

Keywords: triangular barrier, Hartman effect

PACS: 03.65.Xp **DOI:** 10.1088/1674-1056/acf2fe

1. Introduction

As a purely quantum mechanical phenomenon, quantum tunneling is extremely important in a vast range of fields, such as helping overcome the Coulomb barrier in nuclear fusion,[1] tunneling-induced DNA mutation,[2] scanning tunneling microscopes, advanced electronics like tunnel diodes[3] and even false vacuum decay[4,5] in cosmology. With the extensive exploration of quantum tunneling, an early discovered time issue[6,7] is still unresolved; namely, how long does it take for a tunneling particle to traverse a barrier region. Recently, this matter again returned as a bone of contention among researchers,[8–13] mainly thanks to the ultraprecise timing technology developed in attosecond science.[14,15] There are various definitions of tunneling time in the literature, such as Esenbud–Wigner time delay (also termed phase time),[16–18] dwell time[19] and Larmor time.[20–22] Each of them reflects quite distinctive features in quantum tunneling.[23] Aside from the well-studied tunneling times mentioned above, several other time definitions have been proposed. These include the tunneling flight time[10,11] introduced by Rivlin *et al*., the self-adjoint time operator introduced in analogy with the relativistic Dirac Hamiltonian[24] and the entropic time inspired by the statistical implication from the relation between the imaginary Büttiker–Landauer time and the inverse temperature.[25]

With the push from the rapid progress in attosecond science,[26] the question of whether quantum tunneling takes a finite time or is instantaneous seems closer to be answered. Even if it is acknowledged that tunneling takes a finite time, a well-accepted time definition in the academic community is still lacking. For example, phase time keeps track of the peak of a moving wave packet while a thick barrier behaves as a high energy filter, which makes the track of the peak of a wave packet meaningless since it is highly distorted after tunneling; dwell time measures the ratio of the expectation value of a projection operator $\int_{x_\mathrm{i}}^{x_\mathrm{f}} \mathrm{d}x|x\rangle\langle x|$ (the barrier region is included in $[x_\mathrm{i}, x_\mathrm{f}]$) to the incident flux but never distinguishes transmitted waves from reflective partial ones. Many other time definitions, such as Pollack–Miller time[27] or Büttiker–Landauer time,[28] also suffer from various drawbacks, such as the failure to fulfill $\tau_{\mathrm{DW}} = \tau_{\mathrm{T}}|\mathcal{T}|^2 + \tau_{\mathrm{R}}|\mathcal{R}|^2$. In contrast, Larmor time, which maps the time evolution to the rotation angle swept by the spin of an incoming particle in the "clock face" orthogonal to the magnetic field coving the barrier, is not only experimentally feasible[8,9] but also closely related to weak measurement.[29,30] Thus its out-of-plane part corresponds to the back reaction of a measurement.[31,32] Interestingly, the four times can be classified either as the dwell time a particle sojourning in the barrier or the passage time a particle getting across it, and they are neatly unified with the path integral formalisms.[23] These treatments may support that tunneling time can be best viewed as a distribution and thus different definitions only capture specific features of the distribution. In this paper, we mainly focus on the first three well-posed tunneling times and the Larmor time in particular.

As a paradigm in the study of tunneling time, the rectangular barrier draws the most attention and has been analyzed extensively,[33] especially in the discovery of the Hartman effect.[6,7,34] It is proposed that the superluminal behavior arising from the lack of independence of tunneling time on

†Corresponding author. E-mail: spacecraft@pku.edu.cn

© 2024 Chinese Physical Society and IOP Publishing Ltd

the barrier width is an artifact of the misinterpretation[35,36] of phase time as traversal time.[37] This viewpoint receives support from the study of phase and dwell times in a rectangular double barrier and its deformation, double-δ barrier.[38] Later, an analytical study on smooth $A\,\mathrm{sech}^2[x/a]$ barriers showed that a smooth rather than vertical scattering interface indeed alleviates or even smears out the time saturation effect with the increase of barrier width, which is proportional to a, largely due to the steep rising of tunneling rate in a very narrow region in momentum space.[39] Recently, the sech^2-type barrier and well were thoroughly studied in exploring the detail of the reshaping mechanism and the causality issue by analyzing the pole structure of transmission amplitude.[40] Utilizing generalized phase time with time reversal invariance, the Hartman effect in an arbitrary shape with smooth barriers has been studied.[41] A natural example of smooth barriers is the linear gravitational potential, which was first studied by Davies when exploring whether the weak equivalence principle holds in the quantum domain.[42,43] Later on, we proposed a new configuration of magnetic field, spin and momentum of a tunneling particle through the linear potential when analyzing the Larmor time.[44]

In this paper, we extend our previous study of tunneling times in linear potential[44,45] to exact triangular barriers (ETBs), which are barriers with vertical edges either on the left or right side and thus are natural truncations of linear barriers. The major advantage of studying triangular barriers (TBs) is that they can provide analytical solutions. Moreover, TBs have barrier width, height and two side slopes as varying parameters, and these shape parameters facilitate the study of barrier shape sensitivity for various tunneling times. As far as we know, the study of tunneling in TBs was initiated by Fowler and Nordheim to explore the mechanism of electron emission induced by intense electric fields from metals,[46,47] and it is also partially motivated as a rough simplification of the effective potential $V_{\mathrm{eff}}(\boldsymbol{r},\boldsymbol{E}) = -\frac{Ze^2}{r} + e\boldsymbol{E}\cdot\boldsymbol{r} - \alpha^{\mathrm{I}}\frac{\boldsymbol{E}\cdot\boldsymbol{r}}{r^3}$ in laser-induced tunneling ionization.[48] A recent study of the Harman effect through comparisons of tunneling in square and TBs can be found in Refs. [49,50]. Here we mainly compare the phase, dwell and Larmor times for a particle tunneling through a pair of MS ETBs, namely the positive-slope exact triangular barrier (PETB) and the negative-slope exact triangular barrier (NETB). The two kinds of ETBs can be regarded as the two limiting cases of the general TBs. The study of general TBs is in progress. The present study undoubtedly demonstrates the barrier-shape sensitivity of various reflective tunneling times. By defining the velocities associated with these tunneling times, we investigate the Hartman effect further in TBs.

The rest of our paper is organized as follows. In Section 2, we present the basic solution of the Schrödinger equation with TBs and then we demonstrate the basic features of phase, dwell and Larmor "times" in order in Section 3. In Section 4 we define the tunneling velocities associated with phase and Larmor times, and show the barrier width dependence to illustrate the absence of a saturation effect of the tunneling time for TBs. We conclude our results in Section 5.

2. Basic theory of a TB

It is necessary to revisit the one-dimensional tunneling solutions of TBs, which may serve as a simple one-dimensional approximation to the laser-induced tunneling ionization.[14,51] For simplicity, we begin with a PETB, which can be regarded as the truncation of a linear barrier,[44] see Fig. 1(a).

For a particle tunneling through a TB $V_{\mathrm{tri}}(z) = \Theta(z)\Theta(L-z)az$, where a and L are the slope and width of the PETB, respectively. The general solution to the Schrödinger equation

$$\mathrm{i}\hbar\frac{\partial}{\partial t}\Phi(z,t) = \left[-\frac{\hbar^2}{2m}\frac{\partial^2}{\partial z^2} + V_{\mathrm{tri}}(z)\right]\Phi(z,t)$$

is $\Phi(z,t) = \int \mathrm{d}k\,\mathrm{e}^{-\mathrm{i}\hbar k^2 t/2m} g(k)\phi_k(z)$, where the Fourier component $\phi_k(z)$ is the eigensolution of the stationary Schrödinger equation

$$\phi_k''(z) + k^2\left[1 - \frac{2m}{(\hbar k)^2}V_{\mathrm{tri}}(z)\right]\phi_k(z) = 0, \tag{1}$$

and $g(k)$ is the weighting factor in wave number k space for various Fourier components $\phi_k(z)$ of the wave packet $\Phi(z,t)$. To study tunneling time, it is necessary for most of the components $\phi_k(z)$ to tunnel coherently, which means the corresponding transmission rate $T(k)$ does not vary significantly for $|k-k_{\mathrm{c}}| \le \sigma_k$, where k_{c} is the central wave number for the wave packet $\Phi(z,t)$ and σ_k is the width of the wave packet in k space, say, $g(k) = \exp[-\frac{(k-k_{\mathrm{c}})^2}{2\sigma_k^2}]$. For a general barrier, the requirement of a small variation of $T(k)$ in $k \in (k_{\mathrm{c}}-\sigma_k, k_{\mathrm{c}}+\sigma_k)$ means $\sigma_k|\mathrm{d}\log[T(k)]/\mathrm{d}k|_{k=k_{\mathrm{c}}} \ll 1$ and thus it is better to prepare a narrow wave packet in k space.[52] As a preliminary step, in this paper we exclusively discuss eigensolutions, which may be viewed as a nearly chromatic approximation of a narrow wave packet. The wave packet treatment will be left for future works.

Clearly, for a particle outside the region of the TB shown in Fig. 1(a),

$$\phi_k^{\mathrm{i}}(z) \mapsto \alpha\,\mathrm{e}^{\pm\mathrm{i}kz} + \beta\,\mathrm{e}^{\mp\mathrm{i}kz} \quad \text{and} \quad \phi_k^{\mathrm{t}}(z) \mapsto \gamma\mathrm{e}^{\pm\mathrm{i}kz},$$

where the upper or lower sign in $\pm$ depends on whether the particle is injected from the left or right side, and $\phi_k^{\mathrm{i}}(z)$ and $\phi_k^{\mathrm{t}}(z)$ describe the injected and transmitted waves. For a particle inside the region of a PETB, the general solution is

$$\phi_k^b(\tilde{z}) = c_1\mathrm{Ai}[k_a z - \tilde{k}_a^2] + c_2\mathrm{Bi}[k_a z - \tilde{k}_a^2], \tag{2}$$

where c_1, c_2 are the two yet-to-be-determined constants and $L_a \equiv 1/k_a \equiv (2ma/\hbar^2)^{-1/3}$ is a characteristic length scale and

$\tilde{k}_a \equiv kL_a$ is the corresponding dimensionless wave number. By convention, we can always choose the $+$ sign for $\phi_k^{\rm t}(z)$, which is equivalent to assume that the packet is incoming from the left. Exact TBs have two possible configurations, which are related by the spatial reflection $z \mapsto -z$. As an example, the potential in Fig. 1(b) is an NETB, $V_{\rm tri}(-z) = -\Theta(-z)\Theta(L+z)az$, which is MS to its partner in Fig. 1(a).

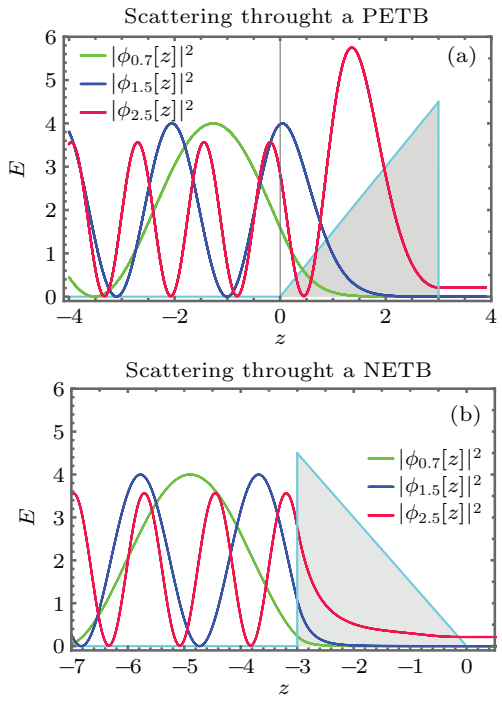


Fig. 1. The probability density distribution $|\phi_k(z)|^2$ for a particle with energy $(\hbar k)^2/(2m)$ tunneling through two spatial MS TBs $V_{\rm tri}(z)$ and $V_{\rm tri}(-z)$. The curves with wave numbers $k = 0.7$, 1.5, 2.5 are depicted with light green, blue and red colors, respectively.

Here we explicitly write down the eigensolution for a PETB in the following and degrade the eigensolutions for the MS NETB and the more general TB in Appendix B. The ansatz for the scattering eigensolution of the PETB $V_{\rm tri}(z)$ is

$$\begin{aligned}\phi_k^{\rm p}(z) &= \phi_k^{\rm i}(z)\Theta(-z) + \phi_k^{b}(z)\Theta(z)\Theta(L-z) \\ &\quad + \phi_k^{\rm t}(z)\Theta(z-L) \\ &= \begin{cases} \alpha\,{\rm e}^{{\rm i}kz} + \beta\,{\rm e}^{-{\rm i}kz}, & z<0, \\ c_{1\rm p}{\rm Ai}[k_a z - \tilde{k}_a^2] + c_{2\rm p}{\rm Bi}[k_a z - \tilde{k}_a^2], & 0<z<L, \\ \gamma\,{\rm e}^{{\rm i}kz}, & L<z. \end{cases} \end{aligned} \tag{3}$$

The continuity equations read

$$\begin{aligned} &\alpha+\beta = c_{1\rm p}{\rm Ai}[-\tilde{k}_a^2] + c_{2\rm p}{\rm Bi}[-\tilde{k}_a^2], \\ &{\rm i}k(\alpha-\beta) = k_a\left(c_{1\rm p}{\rm Ai}'[-\tilde{k}_a^2] + c_{2\rm p}{\rm Bi}'[-\tilde{k}_a^2]\right), \\ &c_{1\rm p}{\rm Ai}[k_aL-\tilde{k}_a^2] + c_{2\rm p}{\rm Bi}[k_aL-\tilde{k}_a^2] = \gamma{\rm e}^{{\rm i}kL}, \\ &\frac{k_a}{{\rm i}k}\left(c_{1\rm p}{\rm Ai}'[k_aL-\tilde{k}_a^2] + c_{2\rm p}{\rm Bi}'[k_aL-\tilde{k}_a^2]\right) = \gamma{\rm e}^{{\rm i}kL}. \end{aligned} \tag{4}$$

For simplicity, we set the incoming flux as a unit such that $\alpha = 1$ and the coefficients can be obtained in a straightforward way as

$$\mathscr{R}_{\rm p} = \frac{2k(k\Omega_0 + {\rm i}k_a\Omega_{\rm c1})}{k^2\Omega_0 + k_a^2\Omega_1 + {\rm i}kk_a\Omega_{\rm c}} - 1, \tag{5}$$

$$\mathscr{T}_{\rm p} = \frac{-2{\rm i}kk_a\,{\rm e}^{-{\rm i}kL}}{\pi\left[k^2\Omega_0 + k_a^2\Omega_1 + {\rm i}kk_a\Omega_{\rm c}\right]}, \tag{6}$$

$$c_{1\rm p} = -\frac{2k\left(k{\rm Bi}[k_aL-\tilde{k}_a^2] + {\rm i}k_a{\rm Bi}'[k_aL-\tilde{k}_a^2]\right)}{k^2\Omega_0 + k_a^2\Omega_1 + {\rm i}kk_a\Omega_{\rm c}}, \tag{7}$$

$$c_{2\rm p} = \frac{2k\left(k{\rm Ai}[k_aL-\tilde{k}_a^2] + {\rm i}k_a{\rm Ai}'[k_aL-\tilde{k}_a^2]\right)}{k^2\Omega_0 + k_a^2\Omega_1 + {\rm i}kk_a\Omega_{\rm c}}, \tag{8}$$

where $\mathscr{R}_{\rm p} \equiv \beta/\alpha$, $\mathscr{T}_{\rm p} \equiv \gamma/\alpha$ are reflective and transmitted amplitudes, respectively, and the subscript p in the coefficients above is for PETBs; similarly the subscript n is for NETBs. We have also defined the following functions:

$$\begin{aligned} \Omega_0 &= {\rm Ai}[k_aL-\tilde{k}_a^2]{\rm Bi}[-\tilde{k}_a^2] - {\rm Ai}[-\tilde{k}_a^2]{\rm Bi}[k_aL-\tilde{k}_a^2], \\ \Omega_1 &= {\rm Ai}'[k_aL-\tilde{k}_a^2]{\rm Bi}'[-\tilde{k}_a^2] - {\rm Ai}'[-\tilde{k}_a^2]{\rm Bi}'[k_aL-\tilde{k}_a^2], \\ \Omega_{\rm c1} &= {\rm Ai}'[k_aL-\tilde{k}_a^2]{\rm Bi}[-\tilde{k}_a^2] - {\rm Ai}[-\tilde{k}_a^2]{\rm Bi}'[k_aL-\tilde{k}_a^2], \\ \Omega_{\rm c2} &= {\rm Ai}'[-\tilde{k}_a^2]{\rm Bi}[k_aL-\tilde{k}_a^2] - {\rm Ai}[k_aL-\tilde{k}_a^2]{\rm Bi}'[-\tilde{k}_a^2], \end{aligned} \tag{9}$$

and $\Omega_{\rm c} = \Omega_{\rm c1} + \Omega_{\rm c2}$. The functions in Eq. (9) are also useful for the eigensolution of the MS NETB, $V_{\rm tri}(-z)$, shown in Fig. 1(b), see Appendix B. The relative probability density profiles for a particle scattering off a pair of MS ETBs in Fig. 1 are quite different. Interestingly, the transmission amplitudes (6) and (B3) are exactly the same, i.e., $\mathscr{T}_{\rm p} = \mathscr{T}_{\rm n}$; the reflection amplitudes (5) and (B2) are closely related, i.e., ${\rm Den}[\mathscr{R}_{\rm p}] = {\rm Den}[\mathscr{R}_{\rm n}]$ and ${\rm Num}[\mathscr{R}_{\rm p}] = ({\rm Num}[\mathscr{R}_{\rm n}\,{\rm e}^{2{\rm i}kL}])^*$, where "Den" and "Num" denote denominator and numerator, respectively, $*$ means the complex conjugate and ${\rm e}^{-2{\rm i}kL}$ is a phase factor due to the coordinate choice. This is only a special case of a general result derived from the one-dimensional stationary Schrödinger equation with the potential $V(z) \in \mathbb{R}$, namely, the transmission amplitudes must be the same and the reflection amplitudes are closely related for a pair of MS barriers $V(z)$ and $V(-z)$, where $V(z)$ can be of an arbitrary shape with a finite nonzero region.[53]

3. The three kinds of tunneling time

3.1. Phase time

Phase time or Eisenbud–Wigner time[16,17,19] is a well-motivated time definition in quantum tunneling, though it lacks essential causality relevance to correlate the transmitted and incoming wave packets and thus cannot capture the elapsed time in the tunneling process.[34] Chasing the peak of a wave packet is useless since a thick barrier works as a high-energy filter and the shape of an incoming wave packet is strongly distorted after tunneling. However, phase time is still a valuable definition in evaluating the time scales in quantum tunneling[38] and reveals the self-interference between the incoming and reflective partial waves. For example, we will see below that the reflective phase times are quite different for a

pair of MS ETBs. The phase times corresponding to reflective and transmitted partial waves are defined below:

$$\begin{aligned}\tau^{\rm R}_{\rm phase} &= \frac{m}{\hbar k}\left(2l_0+\frac{\partial\theta_{\rm R}}{\partial k}\right)\\ &= \frac{m}{\hbar k}\left(2l_0+\frac{\partial\tan^{-1}\left[\frac{{\rm Im}[\mathcal{R}]}{{\rm Re}[\mathcal{R}]}\right]}{\partial k}\right),\end{aligned}\tag{10}$$

$$\begin{aligned}\tau^{\rm T}_{\rm phase} &= \frac{m}{\hbar k}\left(L+\frac{\partial\theta_{\rm T}}{\partial k}\right)\\ &= \frac{m}{\hbar k}\left(L+\frac{\partial\tan^{-1}\left[\frac{{\rm Im}[\mathcal{T}]}{{\rm Re}[\mathcal{T}]}\right]}{\partial k}\right),\end{aligned}\tag{11}$$

where L is the barrier width and l_0 is the spatial distance ahead of the barrier, and $\mathcal{R}$ and $\mathcal{T}$ are the reflection and transmission amplitudes, respectively, say, Eqs. (5) and (6) for a PETB. Also, note that we have ignored the multivaluedness of the tangent function. In other words, we choose the value $\theta_S \in [-\pi/2,\pi/2]$ for the inverse function of "$\theta_S = \tan^{-1}[\tan(\theta_S)]$", where $S = {\rm R}, {\rm T}$.

Since the transmission amplitudes are the same for a pair of MS barriers, such as Eqs. (6) and (B3), the resulting transmitted phase times are also the same. In the following, we do not distinguish the two transmitted phase times (as well as the transmitted Larmor times) provided that the two barriers involved are MS.

To demonstrate the transmitted phase time behavior with the variation of wave number k, we plot $\Delta\tau^{\rm T}_{\rm phase} \equiv \frac{m}{\hbar k}\frac{\partial\theta_{\rm T}}{\partial k}$ and $\tau^{\rm T}_{\rm phase}$ in Fig. 2. From the main figure of $\Delta\tau^{\rm T}_{\rm phase}$, we can see clearly that the transmitted phase time delays are negative for small k, which seems to indicate that it takes less time for a less energetic particle to transverse an ETB than a free spatial region of the same width. In other words, the presence of a barrier seems to speed up instead of slow down the tunneling particle, contradicting the classical intuition, which has long been observed and refined in terms of the famous Hartman effect.[34,38] Another feature shown in the inset of Fig. 2(a) is that the peaks of $\tau^{\rm T}_{\rm phase}(k)$ are shifted to the right and the peak values decrease significantly with the increasing of barrier heights when the barrier width is fixed. In comparison, the peak values of $\Delta\tau^{\rm T}_{\rm phase}$ in the main subfigure reduce very gently with the increase of barrier heights V_0. Compared to $\Delta\tau^{\rm T}_{\rm phase}$, the wave number $\bar{k}$ maximizing $\tau^{\rm T}_{\rm phase}$ or $\Delta\tau^{\rm T}_{\rm phase}$ [i.e., $\max[\tau^{\rm T}_{\rm phase}(k)] = \tau^{\rm T}_{\rm phase}(\bar{k})$], is increasing with increasing V_0, which leads to a further decrease of $\frac{mL}{\hbar\bar{k}}$ in $\tau^{\rm T}_{\rm phase}$. On the other hand, for a fixed barrier height with different barrier widths, the corresponding $\bar{k}$ are roughly the same and the peaks of $\tau^{\rm T}_{\rm phase}(\bar{k})$ or $\Delta\tau^{\rm T}_{\rm phase}(\bar{k})$ increase with increasing barrier width. It looks like $\tau^{\rm T}_{\rm phase}(\bar{k})$ does have a barrier width dependence for TBs, in comparison with the phase time behavior for rectangular barriers, which will be confirmed in Section 4. It is plausible that the occurrence of peaks in $\tau^{\rm T}_{\rm phase}(k)$ for TBs is due to the accumulation of the interference enhanced by the gentle slope either on the left or the right side of the TBs. The peaks in the k-spectrum of the transmitted phase time and the lack of width a independence are also present in the smooth sech$^2(z/a)$-type barrier[39] and may be due to the same interference effect.

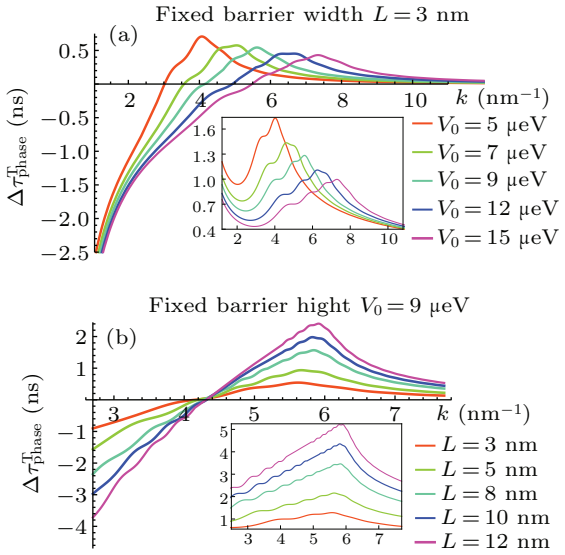


Fig. 2. The transmitted phase time delays $\Delta\tau^{\rm T}_{\rm phase}$ with wave number k for fixed barrier width $L = 3$ nm and barrier height $V_0 \equiv aL = 9$ μV, respectively. The legends with different colors are for different barrier heights in (a) and different barrier widths in (b) and insets, respectively. The units in the vertical and horizontal axes in the insets are exactly the same as the units in the subfigures. (a) The k-spectrum of transmitted phase time delay with fixed barrier width $L = 3$ nm. The inset illustrates the $\tau^{\rm T}_{\rm phase}$ with the same L. (b) The k-spectrum of transmitted phase time delay with fixed barrier height $V_0 = 9$ μV. The inset illustrates the $\tau^{\rm T}_{\rm phase}$ with the same V_0.

Next, we substitute the reflective amplitudes Eqs. (5) and (B2) into Eq. (10) and set the barrier distance $l_0 = 0$. This gives two quite different reflective phase times, $\tau^{\rm R,p}_{\rm phase} = \frac{m}{\hbar k}\frac{\partial\theta^{\rm p}_{\rm R}}{\partial k}$ and $\tau^{\rm R,n}_{\rm phase} = \frac{m}{\hbar k}\frac{\partial\theta^{\rm n}_{\rm R}}{\partial k}$, respectively. Here

$$\theta^{\rm p}_{\rm R} = \tan^{-1}\left[\frac{2kk_a[k_a^2\Omega_1\Omega_{\rm c1} - k^2\Omega_0\Omega_{\rm c2}]}{(k^2\Omega_0)^2 - (k_a^2\Omega_1)^2 + (kk_a)^2\Omega_{\rm c}[\Omega_{\rm c1} - \Omega_{\rm c2}]}\right],\tag{12}$$

$$\theta^{\rm n}_{\rm R} = \tan^{-1}\left[\frac{2kk_a[k_a^2\Omega_1\Omega_{\rm c2} - k^2\Omega_0\Omega_{\rm c1}]}{(k^2\Omega_0)^2 - (k_a^2\Omega_1)^2 + (kk_a)^2\Omega_{\rm c}[\Omega_{\rm c2} - \Omega_{\rm c1}]}\right]\tag{13}$$

are the arguments of the complex reflective amplitudes corresponding to barriers $V_{\rm tri}(z)$ and $V_{\rm tri}(-z)$, respectively. Note that we have subtracted the phase factor e^{-2ikL} due to the nonzero initial position of the potential from $\mathcal{R}_{\rm n}$, see Eq. (B2).

To reveal the dependence of reflective phase times on the norm of slopes, a, of the interface of ETBs, we plot the two-dimensional subfigures of $\tau^{\rm R,p}_{\rm phase}$ and $\tau^{\rm R,n}_{\rm phase}$ with the variation of a and k in Fig. 3, where we keep the barrier area $A = \frac{1}{2}aL^2$ as a constant since the tunneling rate is proportional to $e^{-\frac{2}{\hbar}A}$ in

the Wentzel–Kramers–Brillouin approximation. For PETBs, $\tau^{\mathrm{R,p}}_{\mathrm{phase}}$ decreases with the increase of a, as the increasing slope a means a decrease of $L \propto 1/\sqrt{a}$ and an increase of $V_0 \propto \sqrt{a}$. This means a steeper barrier and a steeper barrier is a more rigid reflector by classical intuitions. The "ridge" of $\tau^{\mathrm{R,p}}_{\mathrm{phase}}$ in Fig. 3(a) decreases and extends to larger k with the increase of a, similarly for $\tau^{\mathrm{R,n}}_{\mathrm{phase}}$. For a fixed a, the phase time peak may be due to the competition tendency of the increasing penetration depth and the increasing velocity of the moving particle caused by the increase of k. When a gets larger, the barrier becomes taller and thinner, and a taller barrier means an incoming particle with the same energy is more likely to be reflected than transmitted and needs more energy to penetrate the same depth in comparison to a barrier with smaller a. This leads to a shift of the peak to larger k and a particle with larger k and a steeper barrier leads to a decrease of the peak value of reflective phase times. The profile of transmitted phase time $\tau^{\mathrm{T}}_{\mathrm{phase}}$ with slope a and wave number k is somewhat similar to $\tau^{\mathrm{R,p}}_{\mathrm{phase}}$ except for quantitative differences.

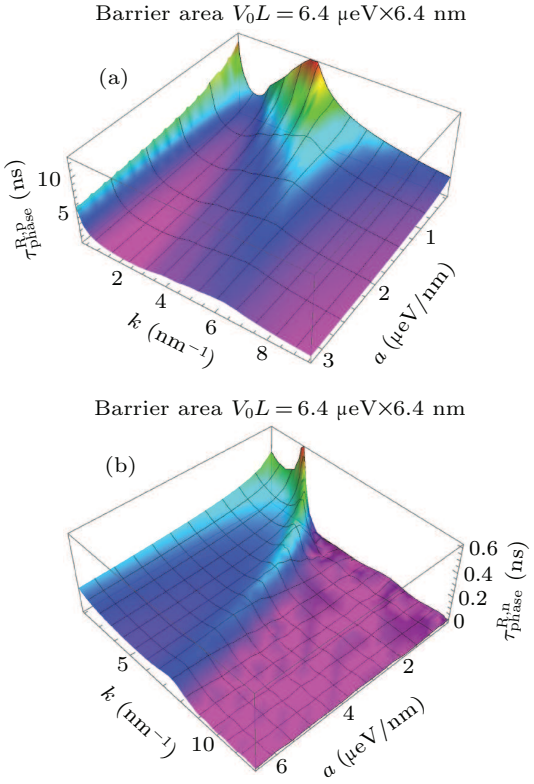


Fig. 3. (a) and (b) The reflective phase times $\tau^{\mathrm{R,p}}_{\mathrm{phase}}$ for $\tau^{\mathrm{R,n}}_{\mathrm{phase}}$ are plotted with varying wave number k and norm of slope a by keeping the product of barrier height and width $V_0L = aL^2 = 6.4 \times 6.4$ μeV·nm a constant, respectively.

In comparison to $\tau^{\mathrm{R,p}}_{\mathrm{phase}}$, the two-dimensional profile of $\tau^{\mathrm{R,n}}_{\mathrm{phase}}$ for NETBs is quite different. The numerical values of $\tau^{\mathrm{R,p}}_{\mathrm{phase}}$ are much larger than those of $\tau^{\mathrm{R,n}}_{\mathrm{phase}}$ when the corresponding parameters k, V_0 and a are the same. This can be easily understood as the slope of a PETB $V_{\mathrm{tri}}(z)$ experienced by a reflective particle is much "softer", while the vertical interface of the mirror symmetric NETB, $V_{\mathrm{tri}}(-z)$, is much stiffer, which acts like a hard wall and reflects the incoming particle much quicker than the "softer" slope of $V_{\mathrm{tri}}(z)$. This can also be verified by the Larmor times. In Fig. 3, we see that the "ridge" of $\tau^{\mathrm{R,n}}_{\mathrm{phase}}$ is much sharper than that of $\tau^{\mathrm{R,p}}_{\mathrm{phase}}$, and the right brink of the ridge of $\tau^{\mathrm{R,n}}_{\mathrm{phase}}$ is a "cliff" instead of the gentle slope as $\tau^{\mathrm{R,p}}_{\mathrm{phase}}$. Moreover, unlike the smooth "plain" on the right side of the ridge of $\tau^{\mathrm{R,p}}_{\mathrm{phase}}$, the right side of the cliff of $\tau^{\mathrm{R,n}}_{\mathrm{phase}}$ is full of sags and crests, a clear signal of interference caused by the two edges of an NETB. For fixed barrier area, a smaller a means the larger characteristic length $L_a \propto a^{-\frac{1}{3}}$ and the larger barrier width L, which allows more constructive interference as L_a, L get more compatible with the wavelength $\lambda = 2\pi/k$, not to mention the zoom-in effect due to the much smaller time scale (an order of magnitude smaller than $\tau^{\mathrm{R,p}}_{\mathrm{phase}}$), thus the interference effect is more transparent in $\tau^{\mathrm{R,n}}_{\mathrm{phase}}$, as shown in Fig. 3.

3.2. Dwell time

In comparison with phase time, dwell time is positively defined and averages over all scattering channels without distinguishing between reflective and transmitted partial waves. Dwell time is defined[54] as

$$\tau_{\mathrm{DW}}[-z_{\mathrm{l}}, L+z_{\mathrm{r}}] \equiv \frac{m}{\hbar k}\int_{-z_{\mathrm{l}}}^{L+z_{\mathrm{r}}} \mathrm{d}z|\phi(k,z)|^2, \tag{14}$$

Substituting the wave function (3) and (B1) into Eq. (14) and for simplicity setting $z_{\mathrm{l}} = z_{\mathrm{r}} = 0$, we can get the dwell times

$$\begin{aligned}\tau^{\mathrm{p}}_{\mathrm{DW}}[0,L] &= \frac{m}{\hbar k}\{(c^*_{1\mathrm{p}}c_{2\mathrm{p}} + c_{1\mathrm{p}}c^*_{2\mathrm{p}})\mathrm{CiI}[L] + |c_{1\mathrm{p}}|^2\mathrm{AiI}[L] \\ &\quad + |c_{2\mathrm{p}}|^2\mathrm{BiI}[L]\}, \end{aligned}\tag{15}$$

$$\begin{aligned}\tau^{\mathrm{n}}_{\mathrm{DW}}[-L,0] &= \frac{m}{\hbar k}\{(c^*_{1\mathrm{n}}c_{2\mathrm{n}} + c_{1\mathrm{n}}c^*_{2\mathrm{n}})\mathrm{CiI}[L] + |c_{1\mathrm{n}}|^2\mathrm{AiI}[L] \\ &\quad + |c_{2\mathrm{n}}|^2\mathrm{BiI}[L]\}, \end{aligned}\tag{16}$$

which are formally the same except for the coefficient c_{1s}, c_{2s} ($s = \mathrm{p}, \mathrm{n}$) differences. Dwell times with an interval $[-z_{\mathrm{l}}, z_{\mathrm{r}}]$ larger than the region of the ETB can be found in Appendix A. The integral of Airy functions, AiI, BiI and CiI are defined as follows:

$$\begin{aligned}\mathrm{AiI}[L] &\equiv \int_0^L \mathrm{d}z\mathrm{Ai}^2[k_a z - \tilde{k}_a^2] \\ &= L_{\mathrm{c}}\left\{(k_aL - \tilde{k}_a^2)\mathrm{Ai1}^2 + \tilde{k}_a^2\mathrm{Ai}^2 + \mathrm{Ai}'^2 - \mathrm{Ai1}'^2\right\}, \\ \mathrm{BiI}[L] &\equiv \int_0^L \mathrm{d}z\mathrm{Bi}^2[k_a z - \tilde{k}_a^2] \\ &= L_{\mathrm{c}}\left\{(k_aL - \tilde{k}_a^2)\mathrm{Bi1}^2 + \tilde{k}_a^2\mathrm{Bi}^2 + \mathrm{Bi}'^2 - \mathrm{Bi1}'^2\right\}, \\ \mathrm{CiI}[L] &\equiv \int_0^L \mathrm{d}z\mathrm{Ai}[k_a z - \tilde{k}_a^2]\mathrm{Bi}[k_a z - \tilde{k}_a^2] \\ &= L_{\mathrm{c}}\left\{(k_aL - \tilde{k}_a^2)\mathrm{Ai1Bi1} + \tilde{k}_a^2\mathrm{AiBi}\right. \\ &\quad \left. + \mathrm{Ai}'\mathrm{Bi}' - \mathrm{Ai1}'\mathrm{Bi1}'\right\}, \end{aligned}\tag{17}$$

where, for notational simplicity, we have defined the abbreviations $\mathrm{Ai} \equiv \mathrm{Ai}[-\tilde{k}_a^2]$, $\mathrm{Bi} \equiv \mathrm{Bi}[-\tilde{k}_a^2]$, $\mathrm{Ai1} \equiv \mathrm{Ai}[k_aL - \tilde{k}_a^2]$, $\mathrm{Bi1} \equiv$

$\mathrm{Bi}[k_aL-\tilde{k}_a^2]$, and the corresponding derivatives $\mathrm{Ai}' \equiv \mathrm{Ai}'[-\tilde{k}_a^2]$, $\mathrm{Bi}' \equiv \mathrm{Bi}'[-\tilde{k}_a^2]$, $\mathrm{Ai1}' \equiv \mathrm{Ai}'[k_aL-\tilde{k}_a^2]$, $\mathrm{Bi1}' \equiv \mathrm{Bi}'[k_aL-\tilde{k}_a^2]$.

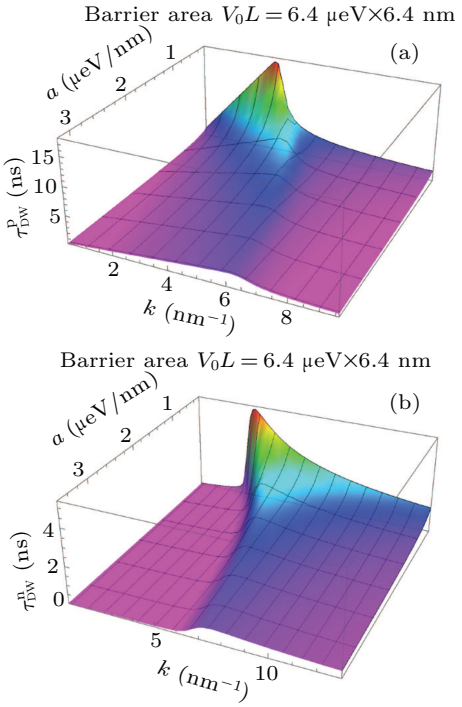


Fig. 4. (a) and (b) The dwell times $\tau^{\mathrm{p}}_{\mathrm{DW}}$ and $\tau^{\mathrm{n}}_{\mathrm{DW}}$ are plotted with varying wave number k and norm of slope a by keeping the barrier area $A = \frac{1}{2}V_0L = 3.2 \times 6.4$ μeV·nm a constant, respectively.

We plot the dwell times with varying wave number k and norm of slope a in Fig. 4. Compared with the reflective phase time $\tau^{\mathrm{R,p}}_{\mathrm{phase}}$, we see that the tendency of $\tau^{\mathrm{p}}_{\mathrm{DW}}$ with varying k is somewhat similar, while the tendency of $\tau^{\mathrm{n}}_{\mathrm{DW}}$ in comparison to $\tau^{\mathrm{R,n}}_{\mathrm{phase}}$ is not. By intuition, the wave number spectrum of the dwell time seems reasonable: if an incoming particle has nearly vanishing kinematical energy in free space, then the probability that the particle dwelling inside the barrier approaches 0 as the barrier becomes impenetrable for a particle with $k \to 0$; moreover, the probability that the particle penetrates beneath the barrier decreases towards zero much faster than k, irrespective of the barrier shape. On the other hand, if k gets larger, it leads to faster velocity and a longer penetration depth and the competition between the two factors will lead to different peak profiles of $\tau^{\mathrm{R,p}}_{\mathrm{DW}}$ and $\tau^{\mathrm{R,n}}_{\mathrm{DW}}$ depending on the barrier shapes. In comparison, the reflective phase times $\tau^{\mathrm{R},s}_{\mathrm{phase}}$ with $s = \mathrm{n,p}$ turn to $+\infty$ with $k \to 0$ since a particle with vanishingly small kinematic energy travels infinitely slowly, which leads to infinitely large reflection times. As for the transmitted phase time delay $\Delta\tau^{\mathrm{T}}_{\mathrm{phase}}$, it diverges to a negative infinite when $k \to 0$, which reflects the growing distortion of the wave packet due to the high-frequency filter effect of thick barriers. This divergence also implies that we can more accurately regard transmitted phase time as a proper time scale estimate in quantum tunneling,[38] but only when the transmitted wave packet is distorted insignificantly in comparison to the incoming packet. Similar to reflective phase times, the numerical values of $\tau^{\mathrm{n}}_{\mathrm{DW}}$ are also much smaller than those of $\tau^{\mathrm{p}}_{\mathrm{DW}}$. Also resembling the phase times shown in Fig. 3, the ridges of the two dwell times become taller and steeper with the decrease of a, as the transmission rate $|\mathcal{T}_{\mathrm{p}}|^2 = |\mathcal{T}_{\mathrm{n}}|^2$ also increases with decreasing a.

For the peak positions in k space when a is fixed, i.e., $\tau^s_{\mathrm{DW}}(\bar{k}) \equiv \max[\tau^s_{\mathrm{DW}}(k)]$, where $s = \mathrm{n,p}$, given a fixed a, each peak of $\tau^{\mathrm{p}}_{\mathrm{DW}}$ locates at a smaller value of k than k_0, i.e., $\bar{k} < k_0$, while for $\tau^{\mathrm{n}}_{\mathrm{DW}}$, $\bar{k} > k_0$. The landscape of the peaks forms the ridge of τ^s_{DW}, $s = \mathrm{n,p}$. Different from the phase time $\tau^{\mathrm{R,n}}_{\mathrm{phase}}$, the cliff of the ridge of $\tau^{\mathrm{n}}_{\mathrm{DW}}$ is on the left side with k slightly smaller than $\bar{k}$ rather than on the right side with slightly larger k. This is because only when an impinging particle's energy is close to the critical value $k_0 \equiv \sqrt{2mV_0}/\hbar$ does it have sufficiently large probability to penetrate beneath the NETB $V_{\mathrm{tri}}(-z)$ due to its steep edge, and hence $\tau^{\mathrm{n}}_{\mathrm{DW}}$ will increase significantly.

As for the smoothness of dwell times in comparison to phase times, the interferences of phase time and interference time may cancel each other due to the relation

$$\tau^{\mathrm{R},s}_{\mathrm{phase}}|\mathcal{R}_s|^2 + \tau^{\mathrm{T}}_{\mathrm{phase}}|\mathcal{T}_s|^2 = \tau^s_{\mathrm{DW}} + \tau^s_{\mathrm{IF}}, \tag{18}$$

which was worked out elegantly by the manipulation of the stationary Schrödinger equation by Winful.[55,56] We now take a closer look at the interference times of negative and positive slope ETBs

$$\tau^s_{\mathrm{IF}} \equiv -\frac{m}{\hbar k^2}\mathrm{Im}[\mathcal{R}_s], \tag{19}$$

where $s = \mathrm{n,p}$ refers to NETB and PETB, respectively. We have subtracted the additional phase factor $\mathrm{e}^{-2\mathrm{i}kL}$ in $\mathcal{R}_{\mathrm{n}}$ to take account of the special coordinate choice $z = -L$ to make Eq. (18) work well when substituting the interference time $\tau^{\mathrm{n}}_{\mathrm{IF}} \propto \mathrm{Im}[\mathcal{R}_{\mathrm{n}}]$ into it. For clearness, we plot τ^s_{IF} in Fig. 5, from which we can see transparently that the oscillatory behavior of $\tau^{\mathrm{p}}_{\mathrm{IF}}(k)$, indicated by the decreasing oscillation amplitudes of the dashed curves with the increase of k, is much larger than that of the interference time $\tau^{\mathrm{n}}_{\mathrm{IF}}(k)$. The curve of $\tau^{\mathrm{n}}_{\mathrm{IF}}(k)$ for either fixed L or V_0 is less zigzagged but the numerical values are comparable to $\tau^{\mathrm{p}}_{\mathrm{IF}}(k)$. However, the smoothness profiles of the dwell times are largely determined by the reflection phase times since the contributions of transmitted phase time $\tau^{\mathrm{T}}_{\mathrm{phase}}|\mathcal{T}_s|^2$ are the same for a pair of MS barriers. As $\tau^{\mathrm{R,p}}_{\mathrm{phase}}$ is relatively smooth and its numerical values are at least an order of magnitude larger than $|\tau^{\mathrm{p}}_{\mathrm{IF}}(k)|$, the ripple caused by the interference time $\tau^{\mathrm{p}}_{\mathrm{IF}}(k)$ can be ignored, which leads to the smooth behavior of $\tau^{\mathrm{p}}_{\mathrm{DW}}$. In comparison, the numerical values of $\tau^{\mathrm{R,n}}_{\mathrm{phase}}$ are of the same order as $\tau^{\mathrm{n}}_{\mathrm{IF}}(k)$, which may cancel each other and give rise to a smooth $\tau^{\mathrm{n}}_{\mathrm{DW}}$.

Similar to phase and dwell times shown previously, both interference times are larger with a smaller norm of slope a, which includes cases of smaller V_0 with fixed L and larger L

with fixed V_0. This is easy to understand as a smaller slope $|a|$ means a steeper barrier and thus less interference between incoming and reflective partial waves. We have shown the two cases in Fig. 5. As a comparison, $\tau^{\rm n}_{\rm IF}(k)$ is more sensitive to the variation of barrier height V_0 with a fixed L, rather than the variation of barrier width L with a fixed V_0. The insensitivity of the latter case can be seen from the nearly coincident solid curves in Fig. 5(b); although they indeed differ slightly, as can be seen in the inset. Taking account of the relation (18) and the smoothness of the dwell times $\tau^{s}_{\rm DW}$ in Fig. 4, we may attribute the general tendency of $\tau^{{\rm R},s}_{\rm phase}$ as being inherited from the dwell time $\tau^{s}_{\rm DW}$. Then, the small oscillatory behavior in $\tau^{{\rm R},s}_{\rm phase}$ can be regarded as the modulation of $\tau^{s}_{\rm DW}$ by the interference time $\tau^{s}_{\rm IF}(k)$.

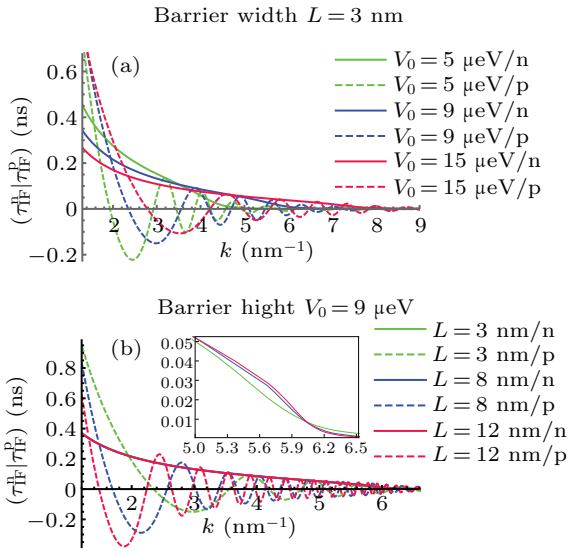


Fig. 5. The interference times $\tau^{s}_{\rm IF}$ [$s = {\rm n}, {\rm p}$ correspond to $V_{\rm tri}(-z)$ and $V_{\rm tri}(z)$, respectively] plotted with wave number k for fixed barrier width $L = 3$ nm and fixed barrier heights $V_0 = 9$ μeV, respectively. The dashed curves correspond to $\tau^{\rm p}_{\rm IF}$ and the solid curves correspond to $\tau^{\rm n}_{\rm IF}$. (a) The $\tau^{s}_{\rm IF}$ for fixed barrier width L. (b) The $\tau^{s}_{\rm IF}$ for fixed barrier height V_0. The inset magnifies the tiny deviation of $\tau^{\rm n}_{\rm IF}$ with three different barrier widths L in the region $k \in (5.0, 6.5)$ nm^{-1}.

3.3. Larmor times

The conventional notion of time refers to a correlation between a certain time-consuming process and the dynamical variable involved, such as the time of a sidereal day and the recording of the rotation of a pointer on a clock face, or the half-life period of the ratio of the number of decayed atoms. Similarly, we can also use some dynamic variables to record the time elapsed in tunneling phenomena. This is the underlying idea for a Larmor clock, where one utilizes the internal degree of freedom, the spin carried by a particle such as a neutron, to determine the time evolved in tunneling. The correlated "pointer" is the angle the spin sweeps on a Bloch sphere.

To make use of a Larmor clock, a small magnetic field is imposed on the region of the ETB only and the Hamiltonian becomes

$$\hat{H}_{\rm tri} = \frac{\hat{\boldsymbol{p}}^2}{2m} + V_{\rm tri}(z) - \boldsymbol{\mu}\cdot\boldsymbol{B}\,\theta(z)\theta(L-z), \tag{20}$$

where $\boldsymbol{\mu} \equiv \hbar\frac{\mu_{\rm N} g}{2}\boldsymbol{\sigma}$ is the magnetic moment and $\mu_{\rm N}$ is the nuclear magneton. The Landé g-factor is $g = -3.826085$ for a neutron. We assume the magnetic field $\boldsymbol{B} = B_0(\sin\theta\cos\phi, \sin\theta\sin\phi, \cos\theta)$. Note that for a full wave packet treatment, the magnetic field is required to cover a larger region[57] than the barrier region $[0,\ L]$, whereas in the monochromatic limit, we only cover the barrier region $z \in [0,\ L]$ with $\boldsymbol{B}$ for simplicity. However, strictly speaking, this naive treatment may violate the uncertainty principle.[58] We adopt the unconventional configuration first proposed in Ref. [44], where the magnetic field $\boldsymbol{B}$ is aligned parallel or antiparallel instead of orthogonal to the direction of motion as conventional configuration of Larmor time in the literature. The ansatz of the wave function is

$$\phi^{\rm p}_k(z) = \begin{cases} \frac{1}{\sqrt{2}}\left[\begin{pmatrix}1\\1\end{pmatrix}{\rm e}^{{\rm i}kz} + \begin{pmatrix}\mathcal{R}^{+}_{\rm p}\\ \mathcal{R}^{-}_{\rm p}\end{pmatrix}{\rm e}^{-{\rm i}kz}\right], & z<0, \\ U\begin{pmatrix} c^{+}_{1\rm p}{\rm Ai}z_0 + c^{+}_{2\rm p}{\rm Bi}z_0 \\ c^{-}_{1\rm p}{\rm Ai}z_1 + c^{-}_{2\rm p}{\rm Bi}z_1\end{pmatrix}, & 0<z<L, \\ \frac{1}{\sqrt{2}}\begin{pmatrix}\mathcal{T}^{+}_{\rm p}\\ \mathcal{T}^{-}_{\rm p}\end{pmatrix}{\rm e}^{{\rm i}kz}, & z>L, \end{cases} \tag{21}$$

where

$$U \equiv \frac{1}{\sqrt{2}}\begin{pmatrix}\cos(\theta/2) & \sin(\theta/2){\rm e}^{-{\rm i}\phi}\\ \sin(\theta/2){\rm e}^{{\rm i}\phi} & -\cos(\theta/2)\end{pmatrix},$$
$$k^2 \equiv \frac{2mE}{\hbar^2} \quad \text{and} \quad k^2_{\pm} \equiv 2m\left(E \pm \frac{\hbar\mu_{\rm N} g B_0}{2}\right)/\hbar^2,$$
$${\rm Ai}z_s \equiv {\rm Ai}\left[k_a z - \tilde{k}^2_a - (-1)^s\frac{mg\mu_{\rm N}B}{\hbar k^2_a}\right],$$
$${\rm Bi}z_s \equiv {\rm Bi}\left[k_a z - \tilde{k}^2_a - (-1)^s\frac{mg\mu_{\rm N}B}{\hbar k^2_a}\right],$$

with $s = 0, 1$ here corresponding to the Airy functions in the upper and lower of the Pauli spinor in Eq. (21), respectively.

Imposing the continuity conditions at $x = 0$ and $x = L$, we can obtain the various coefficients $\mathcal{R}^{\pm}_{\rm p}$, $\mathcal{T}^{\pm}_{\rm p}$ and $c^{\pm}_{1\rm p}$, $c^{\pm}_{2\rm p}$ for a specific θ. For compactness, we degrade the explicit forms of these coefficients in Appendix C, where we include the two cases with $\theta = 0$ and $\theta = \pi$. In the following, we exclusively assume $\theta = 0$ for simplicity. The angle of the spin precession can be obtained from the ratio of the spin expectation values in y and x directions, namely, $\langle\sigma_y\rangle/\langle\sigma_x\rangle$, as the incoming neutron is assumed to be polarized in the x-direction, say $\frac{1}{\sqrt{2}}\begin{pmatrix}1\\1\end{pmatrix}{\rm e}^{{\rm i}kz}$. The precession angle in the x–y plane is $\delta\Phi_c = \tan^{-1}[\langle\sigma_y\rangle_c/\langle\sigma_x\rangle_c]$, where $c = {\rm R}, {\rm T}$ indicate that the expectations are taken on the reflective and transmitted channels, respectively. Substituting the transmitted or reflected partial wave in Eq. (21) into the precession angle $\delta\Phi_c$, the corre-

sponding Larmor time can be obtained as below:

$$\tau^{c}_{\rm LM} = \lim_{B_0\to 0}\frac{\delta\Phi_c}{\omega_L} = \lim_{B_0\to 0}\frac{\tan^{-1}\left[\frac{{\rm i}[\mathcal{I}_c^{-*}\mathcal{I}_c^{+}-\mathcal{I}_c^{+*}\mathcal{I}_c^{-}]}{[\mathcal{I}_c^{-*}\mathcal{I}_c^{+}+\mathcal{I}_c^{+*}\mathcal{I}_c^{-}]}\right]}{g\mu_{\rm N}B_0}, \quad (22)$$

where $\mathcal{I}_c^{\pm} = \mathcal{T}^{\pm}, \mathcal{R}^{\pm}$ correspond to $c = {\rm T}, {\rm R}$ in $\tau^{c}_{\rm LM}$, the transmitted and reflection Larmor times, and $\mathcal{I}_c^{\pm}$ correspond to upper and lower components of the spinor wave function in Eq. (21). The explicit formula for transmitted or reflective Larmor time is given in Appendix C. The procedure to get the Larmor time for the NETB is quite similar, which is also degraded into Appendix C. As already mentioned, the transmitted Larmor time also does not distinguish between a pair of MS barriers, such as ETBs, i.e., $\mathcal{T}_{\rm n}^{\pm} = \mathcal{T}_{\rm p}^{\pm}$, see Eqs. (C2) and (C11). Since the k spectrum of $\tau^{\rm T}_{\rm LM}$ for fixed barrier area is qualitatively similar to that of the dwell times $\tau^{\rm p}_{\rm DW}$ shown in Fig. 4, we do not show them here to avoid redundancy; however, please note that $\tau^{\rm T}_{\rm LM}$ and $\tau^{\rm p}_{\rm DW}$ do differ quantitatively, especially for peak values. Similar to the situation of phase and dwell times shown in Fig. 3 or Fig. 4 for a pair of MS ETBs, $\tau^{\rm R}_{\rm LM,p} \gg \tau^{\rm R}_{\rm LM,n}$ when the wave numbers k are the same. The explicit calculations of $\tau^{\rm R}_{{\rm LM},s} = \lim_{B_0\to 0}\frac{\delta\Phi^{s}_{\rm R}}{g\mu_{\rm N}B_0}$, $(s = {\rm n}, {\rm p})$ can be found in Appendix C, see Eqs. (C9) and (C14). The k spectrums of the Larmor times with fixed barrier width and barrier height are shown in Figs. 6 and 7 for the MS ETBs, respectively. In each of the two figures, we either keep a fixed barrier width L by varying barrier height V_0 and the larger V_0 means the steeper barrier and hence the larger slope a, or we keep a fixed barrier height by varying barrier length and the larger L means the smaller a. Just like phase and dwell times, the reason for $\tau^{\rm R}_{\rm LM,p} \gg \tau^{\rm R}_{\rm LM,n}$ (when the other parameters take the same values) can also be explained by the same fact that, for an incoming particle, the impact interface of the NETB is the vertical wall while that of the PETB is the soft slope. This means that a low-energy particle is immediately bounced back by the hard wall of the NETB, while it has a non-negligible probability to climb up or penetrate beneath the much gentler slope of the PETB. The resultant time in which a particle is bounced back from the PETB is much longer than the same particle impinging on the MS NETB.

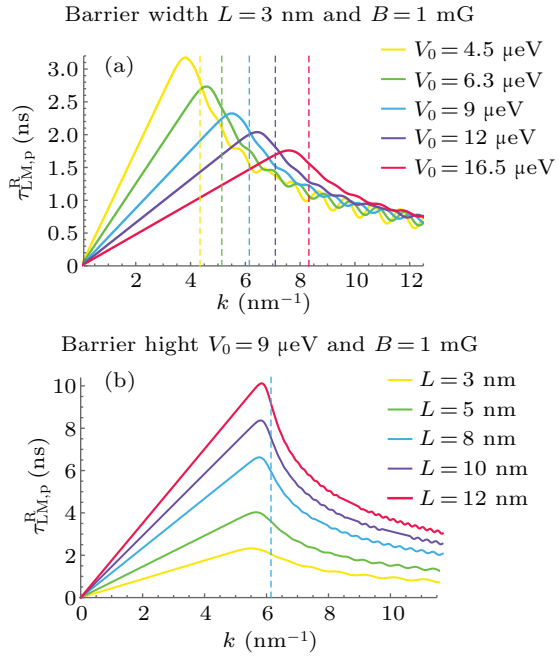


Fig. 6. Reflected Larmor time $\tau^{\rm R}_{\rm LM,p}$ plotted with wave number k for fixed barrier width L and fixed barrier heights V_0, respectively. (a) $\tau^{\rm R}_{\rm LM,p}$ for fixed barrier width $L = 3$ nm. The barrier heights in the legend from top to bottom correspond to slopes $a = 1.5$, 2.1, 3, 4, 5.5 μeV/nm, respectively. (b) $\tau^{\rm R}_{\rm LM,p}$ for fixed barrier height $V_0 = 9$ μeV. The different barrier widths in the legend from top to bottom correspond to slopes $a = 3$, 1.8, 1.125, 0.9, 0.75 μeV/nm, respectively.

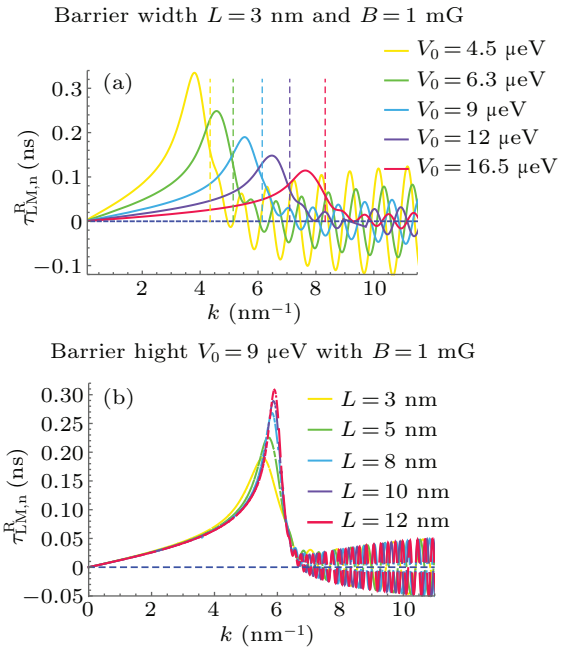


Fig. 7. Reflected Larmor time $\tau^{\rm R}_{\rm LM,n}$ plotted with respect to wave number k for fixed barrier width L and fixed barrier heights V_0, respectively. (a) $\tau^{\rm R}_{\rm LM,n}$ for fixed barrier width $L = 3$ nm. (b) $\tau^{\rm R}_{\rm LM,n}$ for fixed barrier height $V_0 = 9$ μeV.

In comparison with the dwell times shown in Fig. 4, we find that when the wave number k is large enough, either dwell time $\tau^{\rm p}_{\rm DW}$ or $\tau^{\rm n}_{\rm DW}$ get close to the transmitted Larmor time $\tau^{\rm T}_{\rm LM}$. In detail, $\tau^{\rm n}_{\rm DW} \to \tau^{\rm T}_{\rm LM} \leftarrow \tau^{\rm p}_{\rm DW}$ with increasing k when k is larger than k_0. In other words, with increasing k, the dwell times $\tau^{\rm p}_{\rm DW}$ and $\tau^{\rm n}_{\rm DW}$ for the MS ETBs approach the transmitted Larmor time $\tau^{\rm T}_{\rm LM}$ from the upper and lower sides, respectively, which are shown in Fig. 8. To save space, we do not show the curves of the time comparison in k spectrum for the PETB with a fixed barrier height and the curves for the NETB with a fixed barrier width as they lead to the same conclusion; namely, when the wave number k is small enough, the two dwell times approach the corresponding reflective Larmor times, respectively; when k is sufficiently large, the two dwell times approach the transmitted Larmor time from the two opposite sides when the ETBs are MS. This is not unexpected. Since dwell time is a weighted average over transmitted and

reflected partial waves. When k is sufficiently small, the particle is most probably reflected and hence is dominated by the reflected partial wave; on the contrary, when k is large enough, the scattered particle is dominated by the transmitted partial wave, so it is no surprise that dwell time gets close to either the transmitted or reflected Larmor time when k is sufficiently large or small. This fact is shown by the coincidence of the solid curves representing dwell times with the dashed ones representing the corresponding Larmor times in Fig. 8.

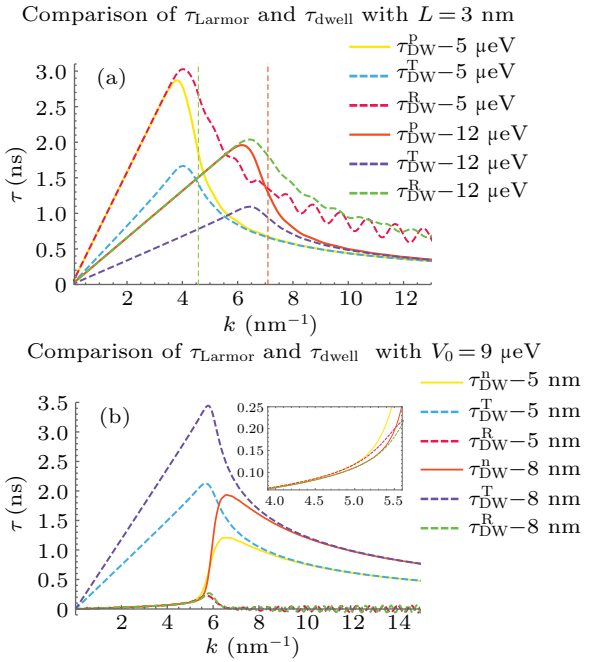


Fig. 8. Comparison of dwell and Larmor times plotted with respect to wave number k. (a) The comparison of $\tau^{\rm p}_{\rm DW}$ with $\tau^{\rm T}_{\rm LM}$ and $\tau^{\rm R}_{\rm LM,p}$ for a PETB when the barrier width L is fixed. (b) The comparison of $\tau^{\rm n}_{\rm DW}$ with $\tau^{\rm T}_{\rm LM}$ and $\tau^{\rm R}_{\rm LM,l}$ for an NETB when the barrier height V_0 is fixed. The inset magnifies the four curves of $\tau^{l}_{\rm DW}$ and $\tau^{\rm R}_{\rm LM,n}$ with two different barrier widths within the region $k\in(3.5,5.5)\times{\rm nm}^{-1}$.

If we ignore small k behaviors and details such as oscillatory behavior, we see that the general tendencies of the reflective Larmor times, $\tau^{\rm R}_{\rm LM,p}$ and $\tau^{\rm R}_{\rm LM,n}$ are somewhat similar to the corresponding ones of the reflective phase times, $\tau^{\rm R,p}_{\rm phase}$ and $\tau^{\rm R,n}_{\rm phase}$. This is not surprising. Falck and Hauge showed that to the zeroth order of the sharp k distribution (close to the monochromatic limit) when one extrapolates the field region into the limit covering only the barrier, the Larmor time reduces to phase time plus extra higher-order corrections, $\mathcal{O}[\omega_{\rm L}^2]$.[57] In the extrapolation limit, the reflective Larmor time is proportional to

$$\int {\rm d}k|g(k)|^2|\mathcal{R}(k)|^2\sin\left[\omega_{\rm L}\tau^{\rm R}_{\rm phase}(k)\right], \tag{23}$$

where $\tau^{\rm R}_{\rm phase}(k)$ is the reflective phase time with mean wave number k. A detailed investigation of the higher-order corrections is much more involved and beyond the scope of this paper. It would be interesting to analyze whether there is a similar relation between phase time and Larmor time in the new configuration with spin and magnetic field,[44] although we may expect that the relation still holds, since the underlying idea is the same as the standard configuration of Larmor time.[20–22] We can also understand the similarity between phase and Larmor times in another way by inspecting the equality derived in Ref. [59]. A complex traversal time was obtained by the Feynman path integral and it was shown that the real part is the Larmor time, which is the partial derivative of the phase of the transmitted or reflected amplitude $\theta_{\rm c}$ to barrier height V_0[59,59] i.e., $\tau^{c}_{{\rm LM},V_0}={\rm Re}\tau^{\Omega}_{c}=-\hbar\partial\theta_c/\partial V_0$ with $c={\rm T,R}$, whereas the phase time is the derivative of the corresponding phase to energy, $\tau^{c}_{\rm phase}=\hbar\partial\theta_c/\partial E$. So $\tau^{c}_{\rm phase}$ measures the response of the phase $\theta_c={\rm arctan}[{\rm Im}[\mathcal{I}_c]/{\rm Re}[\mathcal{I}_c]]$ to the variation of energy E and $\tau^{c}_{\rm LM}$ measures the response of θ_c to the variation of barrier height V_0. Since the variation of V_0 is contrary to the variation of E for a given tunneling probability, there is a minus sign in the definition of $\tau^{c}_{{\rm LM},V_0}$. The resemblance between the definitions may explain certain similarities between $\tau^{\rm R}_{\rm LM,n}$ and $\tau^{\rm R,n}_{\rm phase}$, such as the oscillatory behaviors when k is large enough (e.g., $k>k_0$).

It is interesting to note that the Larmor time $\tau_{{\rm LM},V_0}$ is still different from the transmitted Larmor time $\tau^{\rm T}_{\rm LM}$ defined in Eq. (22). Only when the energy of an incoming particle, $(\hbar k)^2/(2m)$, is well above the barrier height V_0, does $\tau_{{\rm LM},V_0}$ coincide with $\tau^{\rm T}_{\rm LM}$. As an example, note that for a square barrier, $\tau_{\rm DW}=\tau_{{\rm LM},V_0}=-\hbar\partial\arg\mathcal{A}/\partial V_0$, where $\mathcal{A}$ is either the reflective amplitude $\mathcal{R}$ or the transmitted amplitude $\mathcal{T}$, since $\partial\arg\mathcal{T}/\partial V_0=\partial\arg\mathcal{R}/\partial V_0$ for a square barrier, it is a specific example of symmetric barriers;[57] however, the equality $\tau_{\rm DW}=\tau_{\rm LM}$ does not hold for the Larmor time defined in Eq. (22).[44]

4. Saturation effect and the slope dependence of Larmor times

To reveal whether there is a barrier width saturation effect, i.e., the well-known Hartman effect discovered in rectangular barriers,[34] it is necessary to study the L dependence explicitly. The superficial acausality of the Hartman effect relies on two premises: (1) We take it for granted that the tunneling time involved has the meaning of traversal time,[36] a semiclassical concept not necessarily applicable to quantum tunneling, which is a purely quantum mechanical phenomenon without any classical analogy. (2) The saturation of tunneling time with the increase of barrier width leads to an unlimited group velocity of tunneling particle. However, one can view the "apparent acausality" in timing tunneling as a peculiar feature of weak measurement in post-selection of the exponentially suppressed transmitted subensembles from the total ensembles,[31,32,60] and thus it is impossible to utilize tunneling to transfer information[10,11,61] superluminally.

Besides the two points mentioned above, we think that a rectangular barrier with steep edges is too special and it is

necessary to test whether barrier width saturation effect is a common feature in smooth barriers,[39] such as TBs. For this aim, we naively define transmission velocities $v^{\rm T}_{\rm LM} \equiv L/\tau^{\rm T}_{\rm LM}$ and $v^{\rm T}_{\rm phase} \equiv L/\tau^{\rm T}_{\rm phase}$ for transmitted Larmor and phase times, $\tau^{\rm T}_{\rm LM}$ and $\tau^{\rm T}_{\rm phase}$, respectively. For generic TBs, the barrier width is composed of two parts, $L = l_1 + l_2$; however, $\tau^{\rm T}_{\rm LM}$ and $\tau^{\rm T}_{\rm phase}$ only have a slight dependence on the variation of the barrier width separation with given L and V_0, and remains unchanged when the width separations are interchanged, i.e., $l_2 \leftrightarrow l_1$ (for the definition of width separation l_1 and l_2, see Appendix D, and we have excluded TBs with both left and right slopes of the same sign in our considerations). For details, see Eqs. (D6) and (D7). So the equality of $\tau^{\rm T}_{\rm phase}$ as well as the equality of $\tau^{\rm T}_{\rm LM}$ for a pair of MS ETBs are only special/limiting cases of this interchange symmetry $l_2 \leftrightarrow l_1$ of the general TBs when L and V_0 are given.

For velocities corresponding to reflective times, we have to classify the definitions into two classes. For a TB with a positive-slope left edge such as a PETB, we can define reflective Larmor velocity

$$v^{\rm R}_{\rm LM,p} = \theta(k-k_0)\frac{2L}{\tau^{\rm R}_{\rm LM,p}} + \theta(k_0-k)\frac{(\hbar k)^2}{ma\,\tau^{\rm R}_{\rm LM,p}} \tag{24}$$

as well as the reflective phase velocity

$$v^{\rm R,p}_{\rm phase} = \theta(k-k_0)\frac{2L}{\tau^{\rm R,p}_{\rm phase}} + \theta(k_0-k)\frac{(\hbar k)^2}{ma\,\tau^{\rm R,p}_{\rm phase}}. \tag{25}$$

These definitions are in close analogy with the semi-classical picture of a particle reflected by a slope. Likewise, for a generic type of TB (not including those with negative-slope left edges), we can define reflective Larmor or phase times by replacing $\tau^{\rm R}_{\rm LM,p} \mapsto \tau^{\rm R}_{\rm LM,\Delta}$ and $\tau^{\rm R,p}_{\rm phase} \mapsto \tau^{\rm R}_{\rm phase,\Delta}$, where $\tau^{\rm R}_{\rm LM,\Delta}$ and $\tau^{\rm R}_{\rm phase,\Delta}$ are given in Eqs. (D6) and (D7). Increasing the slope of the left edge of a general TB may provide a possible way to define reflection times for NETBs, as an NETB may be viewed as the limiting case of a general TB with the slope of its left edge approaching $+\infty$ while keeping its width and height fixed. However, we take an alternative definition of the reflective Larmor time of an NETB. Since an NETB has an infinite slope acting as a hard wall, we let the weak magnetic field slightly cover a region ahead of this "wall", i.e., in the region $[-l_0,\ L]$, where the barrier takes non-zero values only in the region $[0,\ L]$. The reflective Larmor time is defined as

$$\tau^{\rm R}_{\rm LM,n} = \lim_{B_0\to 0}\frac{{\rm i}\log[\mathcal{R}^{-}_{{\rm n},l_0}/\mathcal{R}^{+}_{{\rm n},l_0}]}{g\mu_{\rm N}B_0}, \tag{26}$$

where $\mathcal{R}^{\pm}_{{\rm n},l_0}$ are the spin-up and -down components of the reflective partial waves and are given by

$$\mathcal{R}^{\pm}_{{\rm n},a} = {\rm e}^{-2{\rm i}kl_0}\frac{\mathcal{C}^{\pm}k_1\cos(k_1l_0) + \left(kK^{\pm}_{\rm d} + {\rm i}k_aK^{\pm}_{\rm cd}\right){\rm i}\sin(k_1l_0)}{\mathcal{D}^{\pm}k_1\cos(k_1l_0) - \left(kK^{\pm}_{\rm s} + {\rm i}k_aK^{\pm}_{\rm cs}\right){\rm i}\sin(k_1l_0)}. \tag{27}$$

The various functions involved are defined by $\mathcal{D}^{\pm} \equiv k^2\Omega^{\pm}_0 + k^2_a\Omega^{\pm}_1 + {\rm i}kk_a\Omega^{\pm}_{\rm c}$, $\mathcal{C}^{\pm} \equiv k^2\Omega^{\pm}_0 - k^2_a\Omega^{\pm}_1 + {\rm i}kk_a(\Omega^{\pm}_{\rm c2} - \Omega^{\pm}_{\rm c1})$, $K^{\pm}_{\rm s} \equiv k^2_1\Omega^{\pm}_0 + k^2_a\Omega^{\pm}_1$, $K^{\pm}_{\rm d} \equiv k^2_1\Omega^{\pm}_0 - k^2_a\Omega^{\pm}_1$, $K^{\pm}_{\rm cs} \equiv k^2\Omega^{\pm}_{\rm c1} + k^2_1\Omega^{\pm}_{\rm c2}$ and $K^{\pm}_{\rm cd} \equiv k^2\Omega^{\pm}_{\rm c1} - k^2_1\Omega^{\pm}_{\rm c2}$.

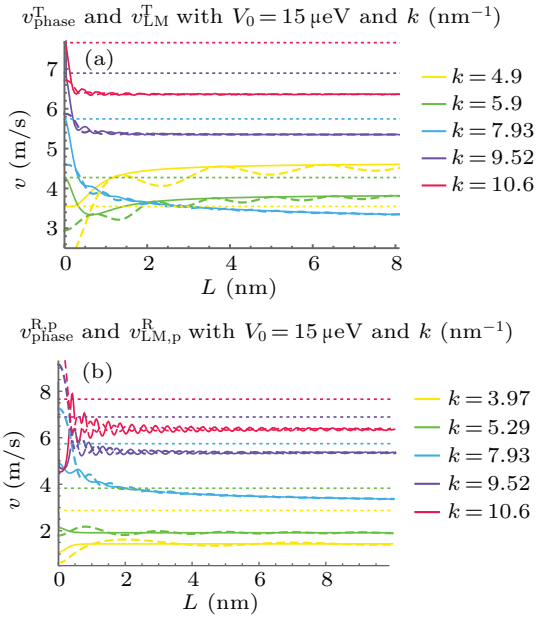


Fig. 9. The barrier width dependence of the velocities defined from the transmitted and reflected Larmor times for PETBs. The dotted lines correspond to free velocities $v_{\rm f}$ and the solid and dashed curves correspond to Larmor and phase velocities, respectively. Note that $k_0 \equiv \sqrt{2mV_0}/\hbar = 7.93$ nm^{-1} represented by the blue lines or curves corresponds to the critical wave number. (a) The $v^{\rm T}_{\rm LM}$ and $v^{\rm T}_{\rm phase}$ with fixed k by varying barrier width L. (b) The $v^{\rm R}_{\rm LM,p}$ and $v^{\rm R,p}_{\rm phase}$ with fixed k by varying barrier width L.

With the above definitions, we will find the barrier width saturation behavior of the tunneling time if the associated velocity increases at least linearly with the increase of barrier width L. First we look at the transmitted and reflective Larmor velocities $v^{\rm T}_{\rm LM}$ and $v^{\rm R}_{\rm LM}$ with a given V_0. From Fig. 9, we see that both velocities approach constants when L is large enough, indicating that there is no barrier width saturation effect for both the transmitted and reflected times for PETBs. In Fig. 9, the horizontal dotted lines are the free velocities $v_{\rm f} \equiv \hbar k/m$ and the wave numbers k shown in the legend with different colors not only correspond to the solid curves, but also to the dotted lines or dashed curves. The solid curves represent the Larmor velocities. It means that for thin PETBs $v^{\rm T}_{\rm LM} < v_{\rm f}$, $v^{\rm R}_{\rm LM} < v_{\rm f}$ and for thick PETBs, only when k is much smaller than the critical $k_0 \equiv \sqrt{2mV_0}/\hbar$ (represented by the dotted yellow and green lines and solid yellow and green curves), the transmitted Larmor velocity $v^{\rm T}_{\rm LM}$ is larger than the free velocity $v_{\rm f}$. This indicates that the presence of a PETB indeed retards the propagation of an incoming particle, unless the energy of the particle is well beneath the apex of the thick PETB, V_0. Further, if $k_1 < k_2$ and $k_1,\ k_2$ are significantly smaller than k_0, $v^{\rm T}_{\rm LM}(k_1) > v^{\rm T}_{\rm LM}(k_2)$. In other words, when k is well inside the tunneling region, the barrier transmission ve-

locity $v^{\rm T}_{\rm LM}(k)$ reverses the order of $v_{\rm f}(k)$, as indicated by the solid yellow and green curves.

The situations for $v^{\rm T}_{\rm phase}$ and $v^{\rm R,p}_{\rm phase}$ are somewhat similar, see the dashed curves in Fig. 9. Roughly speaking, the phase velocities oscillate around the Larmor velocities with the same k, which can be seen clearly from the solid and dashed curves with the same colors in both subfigures. In comparison, the oscillation amplitudes of $v^{\rm R,p}_{\rm phase}$ are much larger than those of $v^{\rm T}_{\rm phase}$ for small L and large $k > k_0$, while for k much smaller than k_0, the variations of $v^{\rm T}_{\rm phase}$ are much larger than those of $v^{\rm R,p}_{\rm phase}$ for thin barriers. The comparison is similar for Larmor velocities. Moreover, the reflective velocities $v^{\rm R,p}_{\rm phase}$ and $v^{\rm R}_{\rm LM,p}$ of PETBs are smaller than and respect orders of free velocities $v_{\rm f}(k)$. This is not surprising, since a positive-slope ETB is like an elastic reflector and thus does retard the propagation of a free particle.

Since we start our timing at a distance l_0 ahead of the steep edge of an NETB and define the reflective Larmor time as in Eq. (26), the reflective Larmor velocity is defined as $v^{\rm R}_{\rm LM,n} \equiv 2l_0/\tau^{\rm R}_{\rm LM,n}$. We plot $v^{\rm R}_{\rm LM,n}$ by varying barrier width L with a fixed slope -8.01 peV/nm and distance $l_0 = 6$ Å, and by varying l_0 with a specific barrier of width $L = 9$ nm and height $V_0 = 45$ peV in Figs. 10(a) and 10(b). The dashed curves correspond to the velocities of free particles with the wave numbers indicated by the colors in the legend. From Fig. 10 we see that the reflective Larmor velocities $v^{\rm R}_{\rm LM,n}$ oscillate around the free velocities $v_{\rm f}$ when k is much smaller than k_0, say $k \leq k_0/2$, and $v^{\rm R}_{\rm LM,n} < v_{\rm f}$ when k is comparatively larger but still in the tunneling region ($k < k_0$), see the blue, purple and red curves. Through inspection of these figures, we find that the NETB only retarded the reflective particle when the corresponding wave number was in the tunneling region but not too small, say $k_0/2 < k < k_0$; $v^{\rm R}_{\rm LM,n}$ also approaches a constant when l_0 is large enough. We may naively think that the increase of $v^{\rm R}_{\rm LM,n}$ with increasing barrier width L in Fig. 10(a) indicates the presence of the barrier width saturation effect in $\tau^{\rm R}_{\rm LM,n}$. However, this is not so simple, as barrier height is also increasing when a is fixed. If instead we increase barrier width L with fixed barrier height, it also leads to an asymptotic constant $v^{\rm R}_{\rm LM,n}$, which may indicate the absence of the barrier width saturation effect for NETBs. In fact, even naively using the phase or Larmor times calculated in the earlier section, Section 3, we may still find that the barrier width saturation behaviors are absent for these reflective times, which is contradictory to the case of rectangular barriers.

A similar behavior can also be observed for TBs with the general shape denoted by $\Delta_{l_1:l_2}$, where the subscript denotes the ratio of the widths separated by the vertical line passing the apex of the triangular barrier, see Appendix D for details. In short conclusion, for transmitted particles, a wide TB seems to accelerate particles' propagation when k is much smaller than k_0, while decelerating it when k is closer to and larger than k_0. However, the situation is the opposite for reflected particles; namely when $k < k_0$, the presence of a wide TB retards the reflection of the reflective particle in comparison to free one. For a TB with $l_1 : l_2 > 1$, only when k is significantly larger than k_0 does the reflected particle go quicker than a free one; while for a TB with steep left slopes, i.e., $l_1 : l_2 < 1$, the reflection velocity acquires a discontinuous jump when $k \geq k_0$. In other words, a wide TB indeed retards the propagation of the reflected particle with $k < k_0$, see Fig. D4. The velocities of a particle scattered off a generic TB are also defined in analogy to Eqs. (24) and (25). Our discussion of TBs with a generic shape is very brief and we will leave the details for future work.

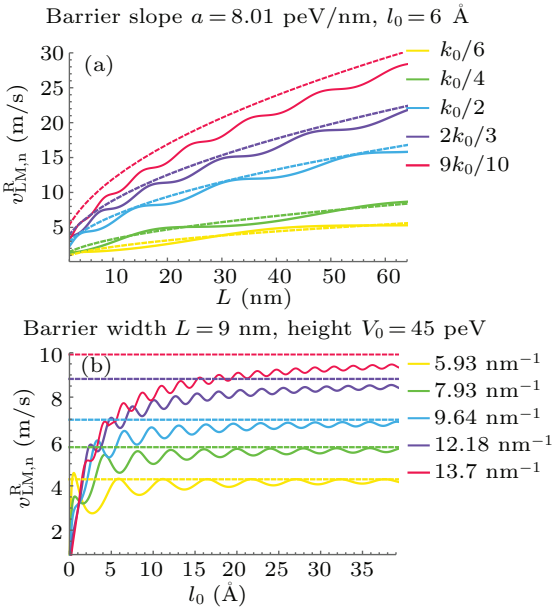


Fig. 10. The dependences of reflective Larmor velocity $v^{\rm R}_{\rm LM,n}$ for NETBs on barrier width L and the barrier distance l_0, respectively. The dashed curves or lines are the corresponding velocities of free particles. (a) The $v^{\rm R}_{\rm LM,n}$ with varying barrier width L of an NETB with a fixed barrier slope -8.01 peV/nm and the barrier distance $l_0 = 6$ Å. (b) The $v^{\rm R}_{\rm LM,n}$ with varying the barrier distance l_0 for an NETB with width $L = 9$ nm and height $V_0 = 45$ peV.

Although we have shown that there is no sign of a barrier width saturation effect through the velocities defined with the phase and Larmor times, the absence of a barrier saturation effect does not necessarily validate that the Larmor or phase times have the traversal time meaning, since we find that when $k \leq k_0$, a larger k means a smaller velocity, in contradiction to the classical intuition that a larger k means a larger velocity, at least in free space.

5. Summary

In this paper, we study the Wigner phase time, Larmor time and dwell time for a particle tunneling through TBs, especially the positive-slope and negative-slope ETBs, abbreviated as PETBs and NETBs, respectively. The transmitted phase or

Larmor times do not distinguish whether the steeper edge is on the left or right side, provided that the pair of TBs are MS. This is simply due to the fact that the transmission amplitudes for a pair of MS one-dimensional barriers are exactly the same, regardless of the barrier shape.

By plotting the dwell, reflective phase and Larmor times as functions of wave number k-spectrum and barrier parameter, such as the slope of a barrier, we demonstrate that these times have quite distinct behaviors for a pair of MS PETBs and NETBs. This may indicate that these times are barrier-shape sensitive. In comparison, dwell time is much smoother than the other two times since it averages over all scattering channels, while the oscillatory behavior of the other two times may be signals of the interference between the transmitted and reflected partial waves scattered by the two edges of a barrier. In short, the tunneling time for an NETB is much smaller than that for an MS PETB given the same wave number k. This may be explained by the fact that a particle with energy lower than barrier height V_0 is more likely and quickly to be reflected by the vertical edge of an NETB than by the soft edge of an MS PETB.

In comparing the oscillatory behaviors of phase and dwell times, we study the well-established relation derived by Winful,[55,56] the Eq. (18). The wave number spectrum of the interference time $\tau^s_{\rm IF}$ ($s={\rm n,p}$) in Fig. 5 reveals that there is indeed slight oscillation in $\tau^{\rm n}_{\rm IF}$ for an NETB than $\tau^{\rm p}_{\rm IF}$ for a PETB, which is expected based on the quite distinct impact edges of an NETB and a PETB. In the comparison of the Larmor and dwell times in Fig. 8, we find that when k is small, dwell time matches the transmitted Larmor time; when k is large, dwell time approaches the reflective Larmor time instead. This fact may be understood by the rough relations expected for dwell time, $\tau^s_{\rm DW} \simeq |{\rm T}|^2\tau^{\rm T}_{{\rm LM},s} + |{\rm R}|^2\tau^{\rm R}_{{\rm LM},s}$, i.e., when k is small, the scattering is dominated by the reflection channel, otherwise it is dominated by transmission channel. This relation also holds approximately for phase time. In fact, Larmor time does equal the phase time for a sharp packet in k space if ignoring higher-order corrections.[57] A detailed investigation of the relation between these times, especially the new configuration of Larmor time,[45] will be meaningful; however, it is beyond our scope and we leave it for future studies.

Finally, by defining velocities with the corresponding phase and Larmor times, we find that the barrier width L saturation effect seems to be absent for TBs. This has been directly demonstrated for PETBs as the velocities approach constants much less than the speed of light in vacuum with increasing L, and similar behaviors are found for NETBs with slightly tedious calculations. However, when L is large enough and k is significantly smaller than k_0, the transmitted velocity $v^{\rm T}_{\rm LM}$ or $v^{\rm T}_{\rm phase}$ can be larger than the velocity of a free particle $v_{\rm f}$ and in contradiction with our intuition, namely, when $k_1 < k_2 < k_0$, $v^{\rm T}(k_1) > v^{\rm T}(k_2)$, where $v^{\rm T}$ refers to either $v^{\rm T}_{\rm LM}$ or $v^{\rm T}_{\rm phase}$. Comparing the reflective velocities $v^{\rm R}_{\rm LM,p}$ and $v^{\rm R}_{\rm phase,p}$ with $v_{\rm f}$, an ETB seems to retard instead of speed up the reflection of a particle. In addition, unlike the transmitted particles, if $k_0 > k_1 > k_2$, $v^{\rm R}(k_1) > v^{\rm R}(k_2)$, see Fig. 9 for details. The situation is similar for a generic shape of TBs and some preliminary results are presented in Appendix D.

The deficiency of our stationary state treatment is that the results may not be fully convincing; however, we can view them as the monochromatic limit of the wave packet method. In short, the main results are summarized as follows. (i) The tunneling times for TBs are barrier-shape sensitive and there seems to be no barrier width saturation effect. (ii) When the energy of the particle is well inside the tunneling region, the transmitted times lose traversal meaning, as supported by the anti-intuitive behaviors from the velocity analysis for ETBs. (iii) When the particle is capable of surpassing the barrier classically, the times may still be meaningful. The temporal behavior of the tunneling process needs to make full use of some novel quantum switch[62,63] or attosecond processes and thus an investigation of tunneling times based on the strict wave packet method is necessary and urgent, and will be explored in the future.

Appendix A: Dwell times for a general interval

The dwell times in the interval $[-z_{\rm l},(z_{\rm r}+L)]$ for a PETB and $[-(z_{\rm l}+L),z_{\rm r}]$ for the MS NETB are

$$\begin{aligned}
&\tau^{\rm p}_{\rm DW}[-z_{\rm l},(z_{\rm r}+L)]\\
&=\frac{m}{\hbar k}\int_{-z_{\rm l}}^{z_{\rm r}+L}{\rm d}z|\phi^{\rm R}_k(z)|^2\\
&=\frac{m}{\hbar k}\Big\{2z_{\rm l}+\frac{|\mathcal{R}_{\rm p}|}{k}[\sin(2kz_{\rm l}+\theta^{\rm p}_\beta)-\sin\theta^{\rm p}_\beta]\\
&\quad+|c_{1{\rm p}}|^2{\rm AiI}[L]+|c_{2{\rm p}}|^2{\rm BiI}[L]\\
&\quad+(c^*_{1{\rm p}}c_{2{\rm p}}+c_{1{\rm p}}c^*_{2{\rm p}}){\rm CiI}[L]+|\mathcal{T}_{\rm p}|^2(z_{\rm r}-z_{\rm l})\Big\},
\end{aligned}\tag{A1}$$

$$\begin{aligned}
&\tau^{\rm n}_{\rm DW}[-(z_{\rm l}+L),z_{\rm r}]\\
&=\frac{m}{\hbar k}\int_{-(z_{\rm l}+L)}^{z_{\rm r}}{\rm d}z|\phi^{L}_k(z)|^2\\
&=\frac{m}{\hbar k}\Big\{\frac{|\mathcal{R}_{\rm n}|}{k}\Big(\sin[2k(z_{\rm l}+L)+\theta^{\rm n}_\beta]-\sin[2kL+\theta^{\rm n}_\beta]\Big)\\
&\quad+2z_{\rm l}+|\mathcal{T}_{\rm n}|^2(z_{\rm r}-z_{\rm l})+|c_{1{\rm n}}|^2{\rm AiI}[L]+|c_{2{\rm n}}|^2{\rm BiI}[L]\\
&\quad+(c^*_{1{\rm n}}c_{2{\rm n}}+c_{1{\rm n}}c^*_{2{\rm n}}){\rm CiI}[L]\Big\},
\end{aligned}\tag{A2}$$

where $\theta^{\rm p}_\beta=\tan^{-1}\left[\frac{{\rm Im}(\mathcal{R}_{\rm p})}{{\rm Re}(\mathcal{R}_{\rm p})}\right]$ and $\theta^{\rm n}_\beta=\tan^{-1}\left[\frac{{\rm Im}(\mathcal{R}_{\rm n})}{{\rm Re}(\mathcal{R}_{\rm n})}\right]$.

Appendix B: Eigen-wave function

The eigensolution $\phi_k(z)$ for a particle tunneling through an NETB, $V_{\rm tri}(-z)=-\Theta(-z)\Theta(L+z)az$, MS to the PETB $V_{\rm tri}(z)$, is

$$\phi_k^N(z) = \phi_k^i(z)\Theta(-z-L) + \phi_k^b(z)\Theta(-z)\Theta(z+L) + \phi_k^t(z)\Theta(z)$$
$$= \begin{cases} \alpha\,\mathrm{e}^{\mathrm{i}kz} + \beta\,\mathrm{e}^{-\mathrm{i}kz}, & z < -L, \\ c_{1l}\mathrm{Ai}[-(k_a z + \tilde{k}_a^2)] + c_{2l}\mathrm{Bi}[-(k_a z + \tilde{k}_a^2)], & -L < z < 0, \\ \gamma\mathrm{e}^{\mathrm{i}kz}, & 0 < z. \end{cases} \tag{B1}$$

From the continuity equations at $z = -L, 0$, we can obtain the solution as below:

$$\mathscr{R}_\mathrm{n} = \mathrm{e}^{-2\mathrm{i}kL}\left[1 - \frac{2k_a(\mathrm{i}k\Omega_{\mathrm{c}1} + k_a\Omega_1)}{k^2\Omega_0 + k_a^2\Omega_1 + \mathrm{i}kk_a\Omega_\mathrm{c}}\right], \tag{B2}$$

$$\mathscr{T}_\mathrm{n} = \frac{-2\mathrm{i}kk_a\,\mathrm{e}^{-\mathrm{i}kL}}{\pi\left[k^2\Omega_0 + k_a^2\Omega_1 + \mathrm{i}kk_a\Omega_\mathrm{c}\right]}, \tag{B3}$$

$$c_{1\mathrm{n}} = \frac{2\,\mathrm{e}^{-\mathrm{i}kL}k\left(k\mathrm{Bi}[-(\frac{k}{k_a})^2] - \mathrm{i}k_a\mathrm{Bi}'[-(\frac{k}{k_a})^2]\right)}{k^2\Omega_0 + k_a^2\Omega_1 + \mathrm{i}kk_a\Omega_\mathrm{c}}, \tag{B4}$$

$$c_{2\mathrm{n}} = \frac{2\,\mathrm{e}^{-\mathrm{i}kL}k\left(\mathrm{i}k_a\mathrm{Ai}'[-(\frac{k}{k_a})^2] - k\mathrm{Ai}[(\frac{k}{k_a})^2]\right)}{k^2\Omega_0 + k_a^2\Omega_1 + \mathrm{i}kk_a\Omega_\mathrm{c}}, \tag{B5}$$

where again we set $\alpha = 1$ and define the reflection and transmission amplitudes as $\mathscr{R}_\mathrm{n} \equiv \beta/\alpha$, $\mathscr{T}_\mathrm{n} \equiv \gamma/\alpha$, respectively.

The eigensolution $\phi_k(z)$ for a particle tunneling through a TB with a general shape $V_\mathrm{tri}(z) = \Theta(l_1+z)\Theta(-z)a(z+l_1) + \Theta(z)\Theta(l_2-z)b(l_2-z)$ is

$$\phi_k^\mathrm{tri}(z) = \begin{cases} \alpha\,\mathrm{e}^{\mathrm{i}kz} + \beta\,\mathrm{e}^{-\mathrm{i}kz}, & z < -l_1, \\ c_{1a}\mathrm{Ai}[k_a(z+l_1) - \tilde{k}_a^2] + c_{2a}\mathrm{Bi}[k_a(z+l_1) - \tilde{k}_a^2], & -l_1 < z < 0, \\ c_{1b}\mathrm{Ai}[-k_b(z-l_2) - \tilde{k}_b^2] + c_{2b}\mathrm{Bi}[-k_b(z-l_2) - \tilde{k}_b^2], & 0 < z < l_2, \\ \gamma\mathrm{e}^{\mathrm{i}kz}, & l_2 < z, \end{cases} \tag{B6}$$

where $al_1 = bl_2 = V_0$, $k_b \equiv (2mb/\hbar^2)^{1/3}$ and $\tilde{k}_b \equiv k/k_b$. From the continuity equations of $\phi_k^\mathrm{tri}(z)$ and $\partial\phi_k^\mathrm{tri}(z)/\partial z$ at coordinates $z = -l_1, 0, l_2$ and the transfer matrix method, we can obtain the transmission and reflection amplitudes

$$\mathcal{T}_\mathrm{tri} = 2kk_ak_b\,\mathrm{e}^{-\mathrm{i}k(l_1+l_2)}/\left[\pi^2\left(2kk_ak_b\Omega_{\mathrm{c}1}^{(a}\Omega_{\mathrm{c}2}^{b)} - \left\{\left[\mathrm{i}k_a(k^2\Omega_0^b\Omega_{\mathrm{c}1}^a + k_ak_b\Omega_1^a\Omega_{\mathrm{c}2}^b) + kk_a^2\Omega_1^a\Omega_0^b\right] + (a \leftrightarrow b)\right\}\right)\right], \tag{B7}$$

$$\mathcal{R}_\mathrm{tri} = \mathrm{i}\,\mathrm{e}^{-2\mathrm{i}kl_1}\frac{\left\{\left[k_b(k_a^2\Omega_1^a\Omega_{\mathrm{c}2}^b - k^2\Omega_0^a\Omega_{\mathrm{c}1}^b) + (a \leftrightarrow b)\right] + \mathrm{i}k\cdot\left[k_b^2\Omega_0^a\Omega_1^b + k_ak_b\Omega_{\mathrm{c}2}^a\Omega_{\mathrm{c}1}^b - (a \leftrightarrow b)\right]\right\}}{\left[2kk_ak_b\Omega_{\mathrm{c}1}^{(a}\Omega_{\mathrm{c}2}^{b)} - \left\{\left[\mathrm{i}k_a(k^2\Omega_0^b\Omega_{\mathrm{c}1}^a + k_ak_b\Omega_1^a\Omega_{\mathrm{c}2}^b) + kk_a^2\Omega_1^a\Omega_0^b\right] + (a \leftrightarrow b)\right\}\right]}, \tag{B8}$$

where as the definitions for the eigensolution of ETBs, we have also defined

$$\begin{aligned}
\Omega_0^i &= \mathrm{Ai}[k_il_i - \tilde{k}_i^2]\mathrm{Bi}[-\tilde{k}_i^2] - \mathrm{Ai}[-\tilde{k}_i^2]\mathrm{Bi}[k_il_i - \tilde{k}_i^2], \\
\Omega_1^i &= \mathrm{Ai}'[k_il_i - \tilde{k}_i^2]\mathrm{Bi}'[-\tilde{k}_i^2] - \mathrm{Ai}'[-\tilde{k}_i^2]\mathrm{Bi}'[k_il_i - \tilde{k}_i^2], \\
\Omega_{\mathrm{c}1}^i &= \mathrm{Ai}'[k_il_i - \tilde{k}_i^2]\mathrm{Bi}[-\tilde{k}_i^2] - \mathrm{Ai}[-\tilde{k}_i^2]\mathrm{Bi}'[k_il_i - \tilde{k}_i^2], \\
\Omega_{\mathrm{c}2}^i &= \mathrm{Ai}'[-\tilde{k}_i^2]\mathrm{Bi}[k_il_i - \tilde{k}_i^2] - \mathrm{Ai}[k_il_i - \tilde{k}_i^2]\mathrm{Bi}'[-\tilde{k}_i^2],
\end{aligned} \tag{B9}$$

and $\Omega_\mathrm{c}^i = \Omega_{\mathrm{c}1}^i + \Omega_{\mathrm{c}2}^i$. The subscript i takes values of a, b for k_i and $1, 2$ for l_i in this section. In the next section, the above definitions can still be useful, only then i takes values of $\pm$ and k_il_i takes the value of k_aL. For the other coefficients c_{1a}, c_{2a}, c_{1b}, c_{2b}, one can set $\alpha = 1$ and substitute $\gamma = \mathcal{T}_\mathrm{tri}$ back into the continuity equations to get the explicit solutions, which will not be given here for brevity. At last, note that the transmission amplitude $\mathcal{T}_\mathrm{tri}$ in Eq. (B7) is symmetric when exchanging k_a, l_1 with k_b, l_2, while the reflection amplitude $\mathcal{R}_\mathrm{tri}$ is not. This implies that the transmission rate and the associated transmission times of TBs are also unaltered under the MS operations by exchanging the pair of a, l_1 and b, l_2 parameters.

Appendix C: The various components in the eigenfunctions in the presence of magnetic fields

The various amplitudes in the eigenfunction for the Larmor time in Eq. (21) are

$$\mathscr{R}_\mathrm{p}^\pm = \frac{2k(k\Omega_0^\pm + \mathrm{i}k_a\Omega_{\mathrm{c}1}^\pm)}{k^2\Omega_0^\pm + k_a^2\Omega_1^\pm + \mathrm{i}kk_a\Omega_\mathrm{c}^\pm} - 1, \tag{C1}$$

$$\mathscr{T}_\mathrm{p}^\pm = \frac{-2\mathrm{i}kk_a\,\mathrm{e}^{-\mathrm{i}kL}}{\pi\left[k^2\Omega_0^\pm + k_a^2\Omega_1^\pm + \mathrm{i}kk_a\Omega_\mathrm{c}^\pm\right]}, \tag{C2}$$

$$c_{1\mathrm{p}}^\pm = -\frac{2k\left(k\mathrm{Bi}[k_aL - \tilde{k}_\pm^2] + \mathrm{i}k_a\mathrm{Bi}'[k_aL - \tilde{k}_\pm^2]\right)}{k^2\Omega_0^\pm + k_a^2\Omega_1^\pm + \mathrm{i}kk_a\Omega_\mathrm{c}^\pm}, \tag{C3}$$

$$c_{2\mathrm{p}}^\pm = \frac{2k\left(k\mathrm{Ai}[k_aL - \tilde{k}_\pm^2] + \mathrm{i}k_a\mathrm{Ai}'[k_aL - \tilde{k}_\pm^2]\right)}{k^2\Omega_0^\pm + k_a^2\Omega_1^\pm + \mathrm{i}kk_a\Omega_\mathrm{c}^\pm}, \tag{C4}$$

when $\theta = 0$. For simplicity, we have defined $\tilde{k}_\pm \equiv \tilde{k}^2 \pm \frac{mg\mu_\mathrm{N}B}{\hbar k_a^2}$. By comparison, it is clear that the amplitudes for a Pauli spinor are totally in parallel to the Eqs. (5)–(8), except the slight shift in the Airy functions. Also note that if setting $\theta = \pi$, the above amplitudes become

$$\mathscr{R}_\mathrm{p}^\pm|_{\theta=\pi} = \mathscr{R}_\mathrm{p}^\mp, \quad \mathscr{T}_\mathrm{p}^\pm|_{\theta=\pi} = \mathscr{T}_\mathrm{p}^\mp, \tag{C5}$$

$$c_{a\mathrm{p}}^+|_{\theta=\pi} = \mathrm{e}^{-\mathrm{i}\phi}c_{a\mathrm{p}}^+, \quad c_{a\mathrm{p}}^-|_{\theta=\pi} = -\mathrm{e}^{\mathrm{i}\phi}c_{a\mathrm{p}}^-, \tag{C6}$$

where $a = 1, 2$. In other words, it looks like that the upper and lower reflective and transmitted amplitudes interchanged when $\theta = 0 \leftrightarrow \theta = \pi$. As for an NETB, since the situation is similar, we do not write the corresponding amplitudes explicitly.

Substituting Eqs. (C1) and (C2) into Eq. (22), we can obtain the explicit formulas for the transmitted and reflective Larmor times, respectively. Substituting Eq. (C5) with the choice of $\theta = \pi$ will lead to equivalent Larmor times and thus will not be shown here. The transmitted Larmor time is

$$\tau_{\rm LM}^{\rm T} = \lim_{B_0\to 0} \frac{\tan^{-1}\left\{\frac{kk_a[\Omega_{\rm c}^+(k^2\Omega_0^- + k_a^2\Omega_1^-) - \Omega_{\rm c}^-(k^2\Omega_0^+ + k_a^2\Omega_1^+)]}{(k^2\Omega_0^- + k_a^2\Omega_1^-)(k^2\Omega_0^+ + k_a^2\Omega_1^+) + (kk_a)^2\Omega_{\rm c}^+\Omega_{\rm c}^-}\right\}}{g\mu_{\rm N}B_0}. \tag{C7}$$

In principle, we can obtain the reflective Larmor time $\tau_{\rm LM,p}^{\rm R}$ in the same way; however, the explicit formula for $\tau_{\rm LM,p}^{\rm R}$ is rather lengthy. To get a more compact formula, we note that $|\mathscr{R}_{\rm p}^+/\mathscr{R}_{\rm p}^-|$ is very close to unity, especially in the limit $B \mapsto 0$. In fact, numerical calculations show that $|\mathscr{R}_{\rm p}^+/\mathscr{R}_{\rm p}^-|^2 - 1 \in [-10^{-4}, 10^{-4}]$ if choosing $k \in [0, 15] \times 10^9$ m^{-1} and $B \in [1, 10^3]$ mG. Since the incoming partial wave is in the σ_x spin eigenstate, i.e., the polar and azimuthal angles $\alpha = \pi/2, \Phi = 0$ on the Bloch sphere, $|\mathscr{R}_{\rm p}^+/\mathscr{R}_{\rm p}^-| \simeq 1$ means that the reflective spin eigenstate still lies in the equator of the Bloch sphere, i.e., $\alpha = \pi/2$, to a good approximation. The precession angle can be read out from the argument of $\mathscr{R}_{\rm p}^+/\mathscr{R}_{\rm p}^-$. In other words, if we define $\mathrm{e}^{\mathrm{i}\delta\Phi_{\rm R}^{\rm p}} \equiv \mathscr{R}_{\rm p}^+/\mathscr{R}_{\rm p}^-$ as an approximation, the precession angle is $\delta\Phi_{\rm R}^{\rm p}$ and the reflective Larmor time is

$$\tau_{\rm LM,p}^{\rm R} = \lim_{B_0\to 0} \frac{\delta\Phi_{\rm R}^{\rm p}}{g\mu_{\rm N}B_0}, \tag{C8}$$

where the subscript p means the Larmor time for PETBs. An explicit form of the precession angle for reflective partial wave is

$$\begin{aligned}\delta\Phi_{\rm R}^{\rm p} = &\left\{\tan^{-1}\left[\frac{kk_a(\Omega_{\rm c1}^+ - \Omega_{\rm c2}^+)}{(k^2\Omega_0^+ - k_a^2\Omega_1^+)}\right]\right.\\ &\left.+\tan^{-1}\left[\frac{kk_a\Omega_{\rm c}^-}{(k^2\Omega_0^- + k_a^2\Omega_1^-)}\right]\right\}\\ &-(+\leftrightarrow -),\end{aligned} \tag{C9}$$

where "$(+\leftrightarrow -)$" means the formal formula in the large brace with the upper indices $+$ and $-$ interchanged. Substituting Eq. (C9) into Eq. (C8), we can get the reflective Larmor time $\tau_{\rm LM,p}^{\rm R}$ for a fermion scattered off the potential $V_{\rm tri}(z)$. Also note that one can utilize $\delta\Phi_{\rm R}^{\rm p} = -\mathrm{i}\log[\mathscr{R}_{\rm p}^+/\mathscr{R}_{\rm p}^-]$ as a simple formal expression.

As for NETBs, when we set $\theta = 0$, the solution is

$$\mathscr{R}_{\rm n}^{\pm} = \mathrm{e}^{-2\mathrm{i}kL}\left[1 - \frac{2k_a(\mathrm{i}k\Omega_{\rm c1}^{\pm} + k_a\Omega_1^{\pm})}{k^2\Omega_0^{\pm} + k_a^2\Omega_1^{\pm} + \mathrm{i}kk_a\Omega_{\rm c}^{\pm}}\right], \tag{C10}$$

$$\mathscr{T}_{\rm n}^{\pm} = \frac{-2\mathrm{i}kk_a\,\mathrm{e}^{-\mathrm{i}kL}}{\pi\left[k^2\Omega_0^{\pm} + k_a^2\Omega_1^{\pm} + \mathrm{i}kk_a\Omega_{\rm c}^{\pm}\right]}, \tag{C11}$$

$$c_{\rm 1n}^{\pm} = \frac{\pm 2\,\mathrm{e}^{-\mathrm{i}kL}k\left(k\mathrm{Bi}[-(\frac{k_\pm}{k_a})^2] - \mathrm{i}k_a\mathrm{Bi}'[-(\frac{k_\pm}{k_a})^2]\right)}{k^2\Omega_0^{\pm} + k_a^2\Omega_1^{\pm} + \mathrm{i}kk_a\Omega_{\rm c}^{\pm}}, \tag{C12}$$

$$c_{\rm 2n}^{\pm} = \frac{\pm 2\,\mathrm{e}^{-\mathrm{i}kL}k\left(\mathrm{i}k_a\mathrm{Ai}'[-(\frac{k_\pm}{k_a})^2] - k\mathrm{Ai}[(\frac{k_\pm}{k_a})^2]\right)}{k^2\Omega_0^{\pm} + k_a^2\Omega_1^{\pm} + \mathrm{i}kk_a\Omega_{\rm c}^{\pm}}. \tag{C13}$$

From Eq. (C11), we see again $\mathscr{T}_{\rm n}^{\pm} = \mathscr{T}_{\rm p}^{\pm}$, so the transmitted Larmor times are the same for MS ETBs, as mentioned already, and hence there is no need to distinguish the transmitted Larmor times by the subscripts p, n in (C7). For the reflective Larmor time $\tau_{\rm LM,n}^{\rm R} = \lim_{B_0\to 0}\frac{\delta\Phi_{\rm R}^{\rm n}}{g\mu_{\rm N}B_0}$, where

$$\begin{aligned}\delta\Phi_{\rm R}^{\rm n} = &\left\{\tan^{-1}\left[\frac{kk_a(\Omega_{\rm c1}^- - \Omega_{\rm c2}^-)}{(k^2\Omega_0^- - k_a^2\Omega_1^-)}\right]\right.\\ &\left.+\tan^{-1}\left[\frac{kk_a\Omega_{\rm c}^-}{(k^2\Omega_0^- + k_a^2\Omega_1^-)}\right]\right\}\\ &-(-\leftrightarrow +).\end{aligned} \tag{C14}$$

The results show that the reflective Larmor time for an NETB is much smaller than the corresponding one for a PETB. In other words, $\tau_{\rm LM,n}^{\rm R}$ is nearly an order of magnitude smaller than $\tau_{\rm LM,p}^{\rm R}$ provided that the relevant parameters are the same.

Appendix D: Some preliminary results for a generic type of TB

With the scattering coefficients such as Eqs. (B7) and (B8), we can obtain tunneling times for a TB with a generic shape by the time definitions shown in the main context. The TB does not include the type of triangle with an obtuse angle on the bottom edge. A sketch of TBs with general shapes and the relative probability densities for a left incoming particle scattered off the barriers is shown in Fig. D1, where the two TBs are MS with barrier height A and width $L = l_1 + l_2$. The widths are separated by the vertical lines (represented by the solid thin lines) passing the apexes to $l_1 : l_2 = 1/2,\ 2/1$ for Figs. D1(a) and D1(b), respectively. Since the calculation of the tunneling times for a TB of generic shape is tedious, we only present the results of the Larmor and phase times directly.

To obtain the Larmor time measured by spin precession, we have to figure out the coefficients in the ansatz similar to Eq. (21) below:

$$\phi_k^{\rm tri}(x) = \begin{cases} \frac{1}{\sqrt{2}}\left[\begin{pmatrix}1\\1\end{pmatrix}\mathrm{e}^{\mathrm{i}kz} + \begin{pmatrix}\mathcal{R}_{\rm tri}^+\\ \mathcal{R}_{\rm tri}^-\end{pmatrix}\mathrm{e}^{-\mathrm{i}kz}\right], & z < -l_1,\\ U\begin{pmatrix}c_{1a}^+\mathrm{Ai}_+^a(z) + c_{2a}^+\mathrm{Bi}_+^a(z)\\ c_{1a}^-\mathrm{Ai}_-^a(z) + c_{2a}^-\mathrm{Bi}_-^a(z)\end{pmatrix}, & -l_1 < z < 0,\\ U\begin{pmatrix}c_{1b}^+\mathrm{Ai}_+^b(z) + c_{2b}^+\mathrm{Bi}_+^b(z)\\ c_{1b}^-\mathrm{Ai}_-^b(z) + c_{2b}^-\mathrm{Bi}_-^b(z)\end{pmatrix}, & 0 < z < l_2,\\ \frac{1}{\sqrt{2}}\begin{pmatrix}\mathcal{T}_{\rm tri}^+\\ \mathcal{T}_{\rm tri}^-\end{pmatrix}\mathrm{e}^{\mathrm{i}kz}, & z > l_2,\end{cases} \tag{D1}$$

where $\mathrm{Ai}_\pm^a(z) \equiv \mathrm{Ai}[k_a(z + l_1) - (\tilde{k}_\pm^a)^2]$ and $\mathrm{Bi}_\pm^a(z) \equiv \mathrm{Bi}[k_a(z + l_1) - (\tilde{k}_\pm^a)^2]$, $\mathrm{Ai}_\pm^b(z) \equiv \mathrm{Ai}[-k_b(z - l_2) - (\tilde{k}_\pm^b)^2]$ and $\mathrm{Bi}_\pm^b(z) \equiv \mathrm{Bi}[-k_b(z - l_2) - (\tilde{k}_\pm^b)^2]$. The $k_{\rm c} \equiv (2mc/\hbar^2)^{\frac{1}{3}}$, $\tilde{k}_\pm^c \equiv \sqrt{\frac{2m}{\hbar^2}(E \pm \mu_z B_0)}/k_{\rm c}$, where the subscript or superscript $c = a,\ b$. With the transfer matrix method, we can get

$$\mathcal{T}_{\rm tri}^{\pm}=\frac{2{\rm i}kk_ak_b\,{\rm e}^{-{\rm i}kL}/\pi^2}{\left[k_a(k_a\Omega_{1\pm}^a+{\rm i}k\Omega_{c1\pm}^a)(k_b\Omega_{c2\pm}^b-{\rm i}k\Omega_{0\pm}^b)\right]+[a\leftrightarrow b]}, \tag{D2}$$

$$\mathcal{R}_{\rm tri}^{\pm}={\rm e}^{-2{\rm i}kl_1}\frac{\left\{\left[k_a(k^2\Omega_{0\pm}^b\Omega_{c1\pm}^a-k_ak_b\Omega_{c2\pm}^b\Omega_{1\pm}^a)+(a\leftrightarrow b)\right]+{\rm i}k\cdot\left[k_a(k_b\Omega_{c1\pm}^a\Omega_{c2\pm}^b+k_a\Omega_{0\pm}^b\Omega_{1\pm}^a)-(a\leftrightarrow b)\right]\right\}}{\left\{\left[k_a\cdot(k_a\Omega_{1\pm}^a+{\rm i}k\Omega_{c1\pm}^a)(k_b\Omega_{c2\pm}^b-{\rm i}k\Omega_{0\pm}^b)\right]+[a\leftrightarrow b]\right\}}. \tag{D3}$$

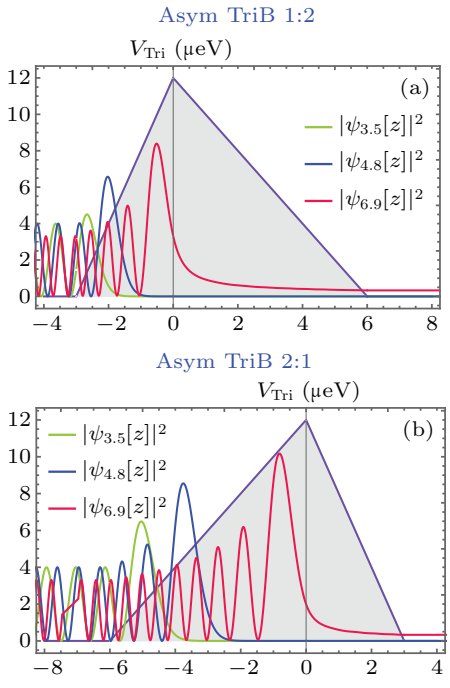


Fig. D1. Sketch map of the probability density distribution $|\psi_k(z)|^2$ for a particle tunneling through a pair of MS TBs with the barrier height A and width separation ratio $l_1:l_2=1/2$ for (a) and $l_1:l_2=2:1$ for (b), where the k are shown in the legends.

Similar to earlier calculations, $\mathcal{T}_{\rm tri}^{\pm}$ is just $\mathcal{T}_{\rm tri}$ if ignoring the sub or superscripts $\pm$, in other words, $\lim_{B_0=0}\mathcal{T}_{\rm tri}^{\pm}=\mathcal{T}_{\rm tri}$. Likewise, $\lim_{B_0=0}\mathcal{R}_{\rm tri}^{\pm}=\mathcal{R}_{\rm tri}$. This is not surprising since a small spin-magnetic field coupling $-\boldsymbol{\mu}\cdot\boldsymbol{B}$ only shifts the barrier either higher or lower a little bit without affecting the form of solutions. Thus, scattering coefficients such as the reflection and transmission amplitudes remain nearly unaltered except for minor changes of parameters, such as $k\mapsto k_\pm$. The angles in the equatorial x–o–y plane swapped by the spin rotation of the transmitted and reflected partial waves relative to the initial spin $\frac{1}{\sqrt{2}}(1,1)^{\rm T}$ pointing in the x-axis can be read from ${\rm e}^{{\rm i}\phi_{\mathcal{T}_{\rm tri}}}\equiv\mathcal{T}_{\rm tri}^{+}/\mathcal{T}_{\rm tri}^{-}$ and ${\rm e}^{{\rm i}\phi_{\mathcal{R}_{\rm tri}}}\equiv\mathcal{R}_{\rm tri}^{+}/\mathcal{R}_{\rm tri}^{-}$, which are

$$\phi_{\mathcal{T}_{\rm tri}}=\tan^{-1}\left[\frac{k_ak\left(k_b\Omega_{c1-}^a\Omega_{c2-}^b-k_a\Omega_{1-}^a\Omega_{0-}^b\right)+(a\leftrightarrow b)}{k_a\left(k^2\Omega_{c1-}^a\Omega_{0-}^b+k_b^2\Omega_{c2-}^a\Omega_{1-}^b\right)+(a\leftrightarrow b)}\right]-[-\leftrightarrow+], \tag{D4}$$

$$\phi_{\mathcal{R}_{\rm tri}}=\tan^{-1}\left[\frac{k\left[k_b(k_a\Omega_{c1+}^b\Omega_{c2+}^a+k_b\Omega_{1+}^b\Omega_{0+}^a)-(a\leftrightarrow b)\right]}{k_a\left(k_ak_b\Omega_{1+}^a\Omega_{c2+}^b-k^2\Omega_{0+}^b\Omega_{c1+}^a\right)+(a\leftrightarrow b)}\right]-(+\leftrightarrow-)+\phi_{\mathcal{T}_{\rm tri}}. \tag{D5}$$

Note that the phase angles $\phi_{\mathcal{T}_{\rm tri}}$, $\phi_{\mathcal{R}_{\rm tri}}$ can be defined in this way as in the case of small B, $\lim_{B_0\mapsto0}|\mathcal{T}_{\rm tri}^{+}/\mathcal{T}_{\rm tri}^{-}|=1$, $\lim_{B_0\mapsto0}|\mathcal{R}_{\rm tri}^{+}/\mathcal{R}_{\rm tri}^{-}|=1$, just as mentioned above in Eq. (C8).

Then we can define the transmitted and reflected Larmor times as

$$\tau_{{\rm LM},\Delta}^{\rm T}=\lim_{B_0\mapsto0}\frac{\phi_{\mathcal{T}_{\rm tri}}}{g\mu_{\rm N}B_0},\quad \tau_{{\rm LM},\Delta}^{\rm R}=\lim_{B_0\mapsto0}\frac{\phi_{\mathcal{R}_{\rm tri}}}{g\mu_{\rm N}B_0}. \tag{D6}$$

As for the phase times, they can be obtained by substituting Eqs. (B7) and (B8) into the definitions (11) and (10), respectively, which leads to

$$\tau_{{\rm ph},\Delta}^{\rm T}=\frac{m}{\hbar k}\frac{\partial\theta_\Delta^{\rm T}}{\partial k},\quad \tau_{{\rm ph},\Delta}^{\rm R}=\frac{m}{\hbar k}\frac{\partial\theta_\Delta^{\rm R}}{\partial k}, \tag{D7}$$

where

$$\theta_\Delta^{\rm T}=\tan^{-1}\left[\frac{k_a(k^2\Omega_0^b\Omega_{c1}^a+k_ak_b\Omega_1^a\Omega_{c2}^b)+(a\leftrightarrow b)}{k\left(k_ak_b\Omega_{c1}^a\Omega_{c2}^b-k_a^2\Omega_1^a\Omega_0^b\right)+(a\leftrightarrow b)}\right], \tag{D8}$$

$$\theta_\Delta^{\rm R}=\tan^{-1}\left[\frac{k^2[(k_a\varpi_1)^2-(a\leftrightarrow b)^2-k^4\varpi_4^2+(k_ak_b)^2\varpi_3^2}{2kk_a(k^2\varpi_1\varpi_4-k_b^2\varpi_2\varpi_3)}\right]. \tag{D9}$$

The four ϖ-s are defined as follows: $\varpi_1\equiv(k_a\Omega_1^a\Omega_0^b-k_b\Omega_{c2}^a\Omega_{c1}^b)$, $\varpi_2\equiv(k_b\Omega_1^b\Omega_0^a-k_a\Omega_{c2}^b\Omega_{c1}^a)$, $\varpi_3\equiv k_b\Omega_{c2}^a\Omega_1^b+(a\leftrightarrow b)$, $\varpi_4\equiv[k_a\Omega_{c1}^a\Omega_0^b+(a\leftrightarrow b)]$. For simplicity, we only show the reflective Larmor times for a pair of asymmetric TBs as a function of wave number k and total width L with the given height of apex $V_0=15$ μeV in Fig. D2. The width separation ratios $l_1:l_2$ of the two triangular barriers are 8 and $1/8$, respectively.

To see whether the phase and Larmor times of TBs are affected by the barrier width saturation effect, we also define the velocities in a fashion similar to those of ETBs defined in Section 4. The results are directly shown in Fig. D3, where we see there are no such effects for general TBs just as for ETBs, since the velocities approach or oscillate around constants when L is large enough. The lack of dashed red curves in Fig. D3 is because the values are much larger than the plot ranges and these curves also oscillate around constants. Moreover, from Fig. D4, we can see that the presence of barriers indeed retarded the propagation of the tunneling particle where the curves are all below the dashed yellow lines representing free particles when $k<k_0$. However, when $k>k_0$, the curves representing barrier width separation ratios 1 : 4 and 1 : 14 all turn to much higher values than the velocities of free particles, while the reflective Larmor or phase velocities for the barriers with much gentler left slopes correspond to $l_1:l_2=4:1$ and 14 : 1 still remains smaller than $v_{\rm f}$ until k is significantly larger than k_0, where oscillation behaviors become transparent both for phase and Larmor velocities. In contrast, the velocities defined with the transmission phase and Larmor times are much

larger than the velocities of the free particles when k is significant smaller than k_0; when k is close or even larger than k_0, the barrier seems retard the propagation of transmitted particles, in contradiction to classical intuitions. Due to space limitations, we leave detailed investigations of the tunneling times for generic shapes of TBs for future works.

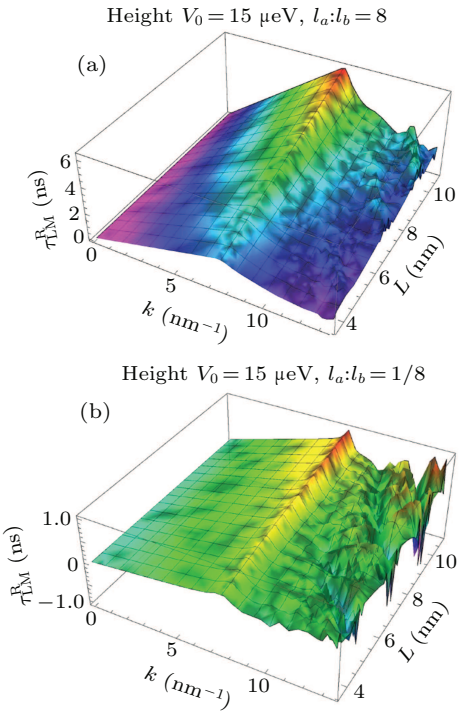


Fig. D2. The reflected Larmor times as functions of the barrier width L and the wave number k of the incoming particle for a pair of MS TBs with width separation ratios (a) 8 : 1 and (b) 1 : 8, respectively.

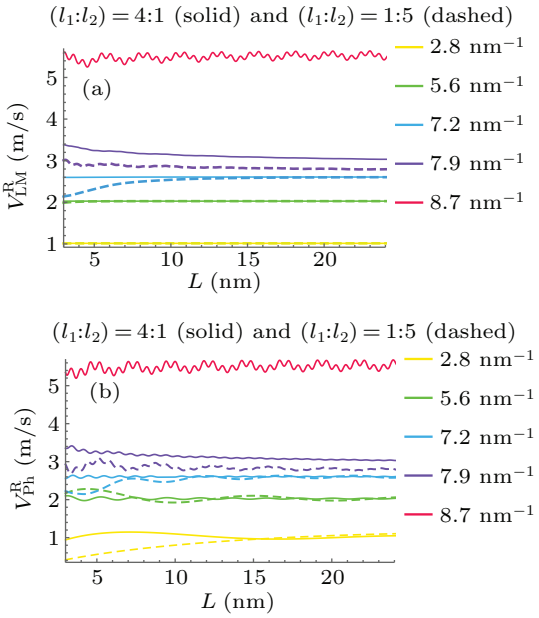


Fig. D3. The reflective velocities defined from the Larmor and phase times for asymmetric TBs with $V_0 = 15$ μeV. The solid and dashed curves in the two subfigures correspond to barrier width separation ratios $l_1 : l_2 = 4 : 1$ and $l_1 : l_2 = 1 : 5$, respectively. The velocities for particles with different wave numbers are shown with different colors in the legends. (a) The reflection Larmor velocities, where the magnetic field is set to be 1 mG. (b) The reflection phase velocities.

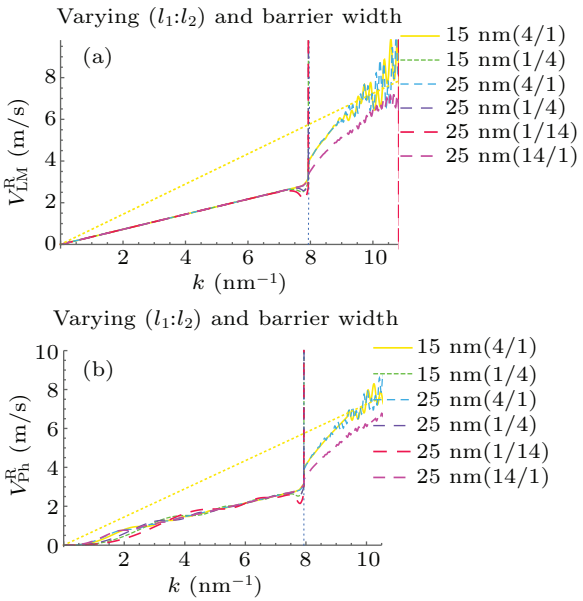


Fig. D4. The comparison of reflective Larmor and phase velocities with the corresponding free particles. The dashed yellow lines correspond to the velocity of free particles and the dotted vertical lines correspond to the critical wave number $k_0 = \sqrt{2mV_0}/\hbar = 7.93$ nm^{-1}. The different colors correspond to barrier width 25 nm and 15 nm with different width separation ratios. (a) The reflection Larmor velocities, where the magnetic field is set to be 1 mG. (b) The reflection phase velocities.

Acknowledgements

Project supported by the National Natural Science Foundation of China (Grant Nos. 11974108, 11875127, and 12211530044) and the Fundamental Research Funds for the Central Universities (Grant No. 2020MS052).

References

[1] Balantekin A B and Takigawa N 1998 *Rev. Mod. Phys.* **77** 70
[2] Golo V L and Volkov V L 2003 *Rev. Mod. Phys.* **131** 14
[3] Britnell L, Gorbachev R V, Jalil R, Belle B D, Schedin F, Mishchenko A, Georgiou T, Katsnelson M I, Eaves L, Morozov S V, Peres N M R, Leist J, Geim A K, Novoselov K S and Ponomarenko L A 2012 *Science* **947** 335
[4] Coleman S 1977 *Phys. Rev. D* **15** 2929
[5] Gen U and Sasaki M 2000 *Phys. Rev. D* **61** 103508
[6] Condon E U and Morse P M 1931 *Rev. Mod. Phys.* **3** 43
[7] Maccoll L A 1932 *Phys. Rev.* **40** 621
[8] Spierings D C and Steinberg A M 2021 *Phys. Rev. Lett.* **127** 133001
[9] Ramos R, Spierings D, Racicot I and Steinberg A M 2020 *Nature* **583** 529
[10] Rivlin T, Pollak E and Dumont R S 2021 *New J. Phys.* **23** 063044
[11] Rivlin T, Pollak E and Dumont R S 2021 *Phys. Rev. A* **103** 012225
[12] Jia L, Xing H and Fu L 2022 *Phys. Rev. A* **105** 062804
[13] Suzuki F and Unruh W G 2023 *Phys. Rev. A* **107** 042216
[14] Landsman A S and Keller U 2015 *Phys. Rep.* **547** 1
[15] Sainadh U S, Xu H, Wang X, Atia-Tul-Noor A, Wallace W C, Douguet N, Bray A, Ivanov I, Bartschat K, Kheifets A, Sang R T and Litvinyuk I V 2019 *Nature* **568** 75
[16] Eisenbud L 1948 *Formal properties of nuclear collisions* (Ph. D. Dissertation) (Princeton)
[17] Wigner E P 1955 *Phys. Rev.* **98** 145
[18] Bohm D 1951 *Quantum Theory* (New York: Prentice-Hall)
[19] Smith F T 1960 *Phys. Rev.* **118** 349
[20] Baz' A I 1967 *Sov. J. Nucl. Phys.* **5** 161
[21] Baz' A I 1967 *Sov. J. Nucl. Phys.* **4** 182
[22] Rybachenko V F 1967 *Sov. J. Nucl. Phys.* **5** 635
[23] Yamada N 2004 *Phys. Rev. Lett.* **93** 170401
[24] Bauer M 2017 *Phys. Rev. A* **96** 022139
[25] Demir D and Güner T 2017 *Ann. Phys.* **386** 291

[26] Han M, Ge P, Wang J, Guo Z, Fang Y, Ma X, Yu X, Deng Y, Wörner H J, Gong Q and Liu Y 2021 *Nat. Photonics* **15** 765
[27] Pollak E and Miller W H 1984 *Phys. Rev. Lett.* **53** 115
[28] Buttiker M and Landauer R 1982 *Phys. Rev. Lett.* **49** 1739
[29] Aharonov Y, Albert D Z and Vaidman L 1988 *Phys. Rev. Lett.* **60** 1351
[30] Aharonov Y and Vaidman L 1990 *Phys. Rev. A* **41** 11
[31] Steinberg A M 1995 *Phys. Rev. Lett.* **74** 2405
[32] Steinberg A M 1995 *Phys. Rev. A* **52** 32
[33] Sokolovski D 2010 *Phys. Rev. A* **81** 042115
[34] Hartman T E 1962 *J. Appl. Phys.* **33** 3427
[35] Winful H G 2003 *Phys. Rev. Lett.* **90** 023901
[36] Winful H G 2006 *Phys. Rev.* **436** 1
[37] Landauer R and Martin Th 1994 *Phys. Rev.* **66** 217
[38] Xiao Z, Huang H and Lu X X 2015 *Int. J. Mod. Phys. B* **29** 1550052
[39] Xiao Z and Huang H 2016 *J. Math. Phys.* **57** 032102
[40] Gutiérrez de la Cal X, Pons M and Sokolovski D 2022 *Sci. Rep.* **12** 3842
[41] Yin C, Wu Z J, Wang X P, Sun J J and Cao Z Q 2010 *Chin. Phys. B* **19** 117305
[42] Davies P C W 1986 *J. Phys. A* **19** 2114
[43] Davies P C W 2005 *Am. J. Phys.* **73** 73
[44] Xiao Z, Zheng S and Liu J C 2021 *J. Phys. B* **54** 105602
[45] Zheng S and Xiao Z 2021 *Adv. Appl. Math.* **10** 1197
[46] Fowler R L and Nordheim L 1928 *Proc. R. Soc. Lond. A* **119** 173
[47] Nordheim L W 1928 *Proc. R. Soc. Lond. A* **121** 626
[48] Pfeiffer A N, Cirelli C, Smolarski1 M, Dimitrovski D, Abu-samha M, Madsen L B and Keller U 2012 *Nat. Phys.* **8** 76
[49] Jensen K L, Riga J, Lebowitz J L, Seviour R and Shiffler D A 2022 *Proc. R. Soc. Lond. A* **132** 124303
[50] Jensen K L, Shabaev A, Riga J, Shiffler D A, Lebowitz J L and Seviour R 2021 *Phys. Rev. A* **104** 062203
[51] Camus N, Yakaboylu E, Fechner L, Klaiber M, Laux M, Mi Y, Hatsagortsyan K Z, Pfeifer T, Keitel C H and Moshammer R 2017 *Phys. Rev. Lett.* **119** 023201
[52] Though to have a better resolution of time issue, it is also necessary to require the spread of the wave packet in coordinate space to be much smaller than the barrier width, which means that the spread σ_k in k space cannot be too narrow.
[53] Cohen-Tannoudji C, Diu B and Laloe F 2019 *Quantum Mechanics* Vol. 1 (Wiley-VCH)
[54] Büttiker M 1983 *Phys. Rev. B* **27** 6178
[55] Winful H G 2003 *Phys. Rev. Lett.* **91** 260401
[56] Winful H G, Ngom M and Litchinitser N M 2004 *Phys. Rev. A* **70** 052112
[57] Falck J P and Hauge E H 1988 *Phys. Rev. B* **38** 3287
[58] Hauge E H and Støvneng J A 1989 *Rev. Mod. Phys.* **61** 917
[59] Sokolovski D and Baskin L M 1987 *Phys. Rev. A* **36** 4604
[60] Sokolovski D, Msezane A Z and Shaginyan V R 2005 *Phys. Rev. A* **71** 064103
[61] Dumont R S, Rivlin T and Pollak E 2000 *New J. Phys.* **22** 093060
[62] Zhou L, Gong ZR, Liu Y X, Sun C P and Nori F 2008 *Phys. Rev. Lett.* **101** 100501
[63] Zhou L, Dong H, Liu Y X, Sun C P and Nori F 2008 *Phys. Rev. A* **78** 063827